Acta Biomaterialia xxx (xxxx) xxx

Contents lists available at ScienceDirect

Acta Biomaterialia

journal homepage: www.elsevier.com/locate/actbio

Review article

State-of-the-art and tomorrow's challenges and opportunities in constitutive modeling of soft biological tissues with a focus on arterial, cardiac and brain biomechanics

Stéphane Avril [a], Alain Goriely [b], Gerhard A. Holzapfel [c,d,*], Ellen Kuhl [e], David Nordsletten [f], Ray W. Ogden [g]

[a] Mines Saint-Etienne, Université Jean Monnet Saint-Etienne, INSERM, SAINBIOSE U1059, Saint-Etienne, France
[b] Mathematical Institute, University of Oxford, UK
[c] Institute of Biomechanics, Graz University of Technology, Austria
[d] Department of Structural Engineering, Norwegian University of Science and Technology (NTNU), Trondheim, Norway
[e] Department of Mechanical Engineering, Stanford University, USA
[f] Department of Biomedical Engineering, University of Michigan, Ann Arbor, USA
[g] School of Mathematics and Statistics, University of Glasgow, UK

ARTICLE INFO

Keywords:
Biomechanics
Mechanobiology
Constitutive modeling
Heart
Brain
Artery

ABSTRACT

The aim of this paper is to provide an up-to-date overview of the constitutive modeling of soft biological tissues, both from a simulation and experimental perspective by taking into account different length scales. After providing some essential ingredients on continuum mechanics, especially nonlinear elasticity, the focus is on mechanical and structural modeling of fiber-reinforced materials, including the features of soft tissues such as collagen fiber dispersion, and residual stresses. Materials testing and data acquisition for constitutive modeling of soft tissue are also discussed, with emphasis on measuring strain fields using imaging techniques and digital image correlation. The topics are illustrated for three tissues. First, applications to arteries are illustrated and the effects of vascular adaptation in diseases such as aneurysms and aortic dissections are discussed. The second application includes cardiac biomechanical modeling, touching on the nonlinear anisotropic and viscoelastic nature of the myocardium, the synthesis and integration of these concepts into whole-organ models, and the assimilation of image-based data for patient-specific modeling. The third focus is on brain mechanics, including the unusual response of brain tissues and axons under loads, the formation of the brain and skull during development, and the study of brain trauma and diseases. The important area of machine learning for discovering constitutive models and parameter identification is also covered. To show how constitutive models can be selected, a model discovery approach is reviewed. Because the mechanical properties of soft tissues may vary with age, sex, health and disease an account of uncertainty quantification in the model assumptions and measurement errors is provided. Future directions and challenges for research in multiscale biomechanics and mechanobiology are identified involving mechanical, biological, electrical and fluid–structure interactions.

Statement of Significance:

This review provides a state-of-the art summary of the importance of constitutive modeling, simulations and their experimental basis of soft biological tissues. A focus is put on applications to materials testing and data acquisition, artery and cardiac biomechanics and mechanobiology at different length scales and the biomechanics of brain at the cell, tissue and organ levels. In addition, novel approaches to constitutive modeling and parameter identification of soft biological tissues based on machine learning, model discovery and data mining are highlighted. Finally, open problems are summarized and recent and future directions and challenges for research in multiscale biomechanics and mechanobiology are identified, particularly involving mechanical, biological, electrical and fluid–structure interactions.

* Corresponding author at: Institute of Biomechanics, Graz University of Technology, Austria.
E-mail address: holzapfel@tugraz.at (G.A. Holzapfel).

https://doi.org/10.1016/j.actbio.2026.02.022
Received 27 October 2025; Received in revised form 24 January 2026; Accepted 12 February 2026
Available online 14 February 2026

1. Introduction

This paper provides a review following the 10th version in 2023 of the Summer Schools in Biomechanics that have been organized in the series that started in 2001. The topics covered in the summer school are reflected in the contents of the paper. The underlying theme is to focus on the constitutive modeling and computational biomechanics of soft tissues specifically artery walls, the myocardium and the brain.

The detailed content of the paper is outlined as follows. Section 2 summarizes the essential continuum mechanics required for applications in the subsequent sections. The deformation, stress and the theory of hyperelasticity and constitutive laws for fiber-reinforced materials are presented. Section 3 deals with material testing techniques and the associated stress–strain data acquisition for soft biological tissues required for the constitutive modeling. In particular, the *in vitro* statically determinate and indeterminate material testing are discussed followed by *in vivo* testing. Recent trends are highlighted, in particular the combination of mechanical tests with microscopic imaging of the tissue structure. Section 4 is dedicated to the first application in the field of soft tissue, namely arterial walls. In particular, the structural and functional relationships are examined. Current findings on the microstructure and biomechanical behavior of arterial walls are presented, and both the passive and active states of the wall are described. Constitutive models for both states are then described, with a focus on modeling the collagen fiber structure and the related dispersion, as these have a significant influence on the mechanical response of the vascular walls. Possible future trends for a better implementation of computational biomechanics in clinics for personalized diagnosis and treatment of pathologies are presented. Section 5 deals with the second soft tissue application towards the biomechanical and mechanobiological modeling of the heart with particular reference to cardiac mechanics across scales—from the cellular level to the whole heart. Also this section closes with a discussion on recent trends and future directions such as personalized digital twins and patient-specific modeling characteristics that capture cardiac behavior over time or the use of engineered heart tissues for understanding cardiac mechanics. The final application concerns the biomechanics of brain tissue (Section 6). We discuss brain biomechanics specifically at the cellular, tissue, and organ levels. Traditionally, the brain was considered as isolated from mechanical influences, but it is now known to be profoundly affected by mechanical processes at all levels—from cellular-level mechanosensing in neuronal development and synaptic function, to tissue-level viscoelastic responses, to organ-level phenomena such as cortical folding and trauma-induced swelling. We show how recent advances, including multiscale modeling, novel constitutive laws, and data-driven approaches, are changing our understanding of brain biomechanics and opening new avenues for the diagnosis, modeling, and treatment of neurological disorders.

Section 7 addresses machine learning and data mining in the context of constitutive modeling of soft biological tissues. After a brief overview of the use of classical neural networks for learning constitutive models, we introduce the concept of constitutive neural networks with build-in physical and thermodynamic constraints. We discuss how we can leverage constitutive neural networks to automatically discover models and parameters that best fit soft tissue data. We show how to sparsify the discovered models to make them generalizable and interpretable. Finally, we overlay uncertainty to determine not only point values for the model parameters but also means and credible intervals, which allow us to quantify model uncertainty. The concluding section identifies some future directions of research in multiscale biomechanics and mechanobiology, and the associated challenges that are involved the mechanical, biological, electrical and fluid–structure interactions.

2. Continuum mechanics preliminaries

2.1. Geometry and deformation

For general background underlying the theory summarized in the following sections we refer to the books [1,2].

In three dimensions the *material points* of a solid continuum are represented by position vectors denoted $\mathbf{X}$ in a fixed configuration. This is referred to as the *reference configuration*, which is denoted $\mathrm{B_r}$. Its boundary is denoted $\partial\mathrm{B_r}$. When external forces (with surface and body contributions) are applied to the continuum it is deformed and takes up a *deformed configuration*. This is denoted B, wherein $\mathbf{X}$ now sits at $\mathbf{x}$. The boundary of B is denoted ∂B. The deformation from $\mathrm{B_r}$ to B is characterized by the vector function χ, so that

$$\mathbf{x} = \chi(\mathbf{X}) \quad \text{for all } \mathbf{X} \in \mathrm{B_r}. \tag{1}$$

Its inverse is $\mathbf{X} = \chi^{-1}(\mathbf{x})$, which applies for all $\mathbf{x} \in$ B. It is required that $\chi(\mathbf{X})$ is suitably regular. Time is not included explicitly in the current development.

We represent the mechanical properties of the material by various scalar, vector and tensor fields. These are expressed in either Lagrangian or Eulerian forms, i.e. as functions of $\mathbf{X}$ in $\mathrm{B_r}$ or as functions of $\mathbf{x}$ in B, respectively. For illustration, a scalar function, say $\phi(\mathbf{x})$ based on B (Eulerian) may equally be represented as $\Phi(\mathbf{X})$ (Lagrangian) using (1) to arrive at

$$\phi(\mathbf{x}) = \phi[\chi(\mathbf{X})] \equiv \Phi(\mathbf{X}), \tag{2}$$

and conversely, by using the inverse of (1).

We denote by $\mathbf{F}$ the so-called *deformation gradient*, which is given by

$$\mathbf{F}(\mathbf{X}) = \mathrm{Grad}\,\mathbf{x} \equiv \mathrm{Grad}\,\chi(\mathbf{X}), \tag{3}$$

wherein Grad represents the gradient operator based on $\mathrm{B_r}$, i.e. with respect to $\mathbf{X}$. As is usual, we denote the determinant $\det\mathbf{F}$ by J, which is positive by convention. For an incompressible material the constraint $J = 1$ must be satisfied at all points $\mathbf{X} \in \mathrm{B_r}$.

From $\mathbf{F}$, two special symmetric tensors are formed, namely the *right Cauchy–Green deformation tensor*, denoted $\mathbf{C}$ and its left counterpart, denoted $\mathbf{b}$. In terms of $\mathbf{F}$ these are given by

$$\mathbf{C} = \mathbf{F}^{\mathrm{T}}\mathbf{F}, \quad \mathbf{b} = \mathbf{F}\mathbf{F}^{\mathrm{T}}, \tag{4}$$

respectively, $(\bullet)^{\mathrm{T}}$ being the transpose of $(\bullet)$. Note that $\det\mathbf{C} = \det\mathbf{b} = J^2$. A related kinematic quantity is the *stretch*, denoted λ associated with a direction $\mathbf{M}$ (a unit vector dependent on position $\mathbf{X}$ in $\mathrm{B_r}$). This is defined by

$$\lambda(\mathbf{M}) = [\mathbf{M} \cdot (\mathbf{C}\mathbf{M})]^{1/2}. \tag{5}$$

If the direction $\mathbf{M}$ is unstretched then $\lambda(\mathbf{M}) = 1$ for all $\mathbf{C}$. We require that $0 < \lambda(\mathbf{M}) < \infty$.

The important *polar decomposition theorem* allows $\mathbf{F}$ to be written as either of the products

$$\mathbf{F} = \mathbf{R}\mathbf{U} = \mathbf{V}\mathbf{R}, \tag{6}$$

wherein $\mathbf{R}$ is a rotation tensor, $\mathbf{U}$ is the right stretch tensor and $\mathbf{V}$ is the left stretch tensor, both of which are symmetric and positive definite.

The symmetry and positive definiteness of $\mathbf{U}$ ensures that it has mutually orthonormal eigenvectors, here denoted $\mathbf{u}^{(i)}$, and associated strictly positive eigenvalues, say λ_i. Thus, $\mathbf{U}\mathbf{u}^{(i)} = \lambda_i\mathbf{u}^{(i)}$, $i = 1, 2, 3$. Moreover, the spectral decomposition of $\mathbf{U}$ follows as

$$\mathbf{U} = \sum_{i=1}^{3} \lambda_i \mathbf{u}^{(i)} \otimes \mathbf{u}^{(i)}. \tag{7}$$

The left stretch tensor $\mathbf{V}$ has the same eigenvalues λ_i, and from the polar decomposition theorem it follows that its eigenvectors, denoted $\mathbf{v}^{(i)}$, are related to $\mathbf{u}^{(i)}$ via $\mathbf{v}^{(i)} = \mathbf{R}\mathbf{u}^{(i)}$.

From the general definition of stretch (5) we have $\lambda_i = \lambda(\mathbf{u}^{(i)})$. The λ_i are referred to as the *principal stretches* associated with the eigenvectors $\mathbf{u}^{(i)}$ and $\mathbf{v}^{(i)}$ (the Lagrangian and Eulerian principal directions, respectively).

2.2. Nominal and Cauchy stress tensors

Let $\mathbf{b}$ be the body force per unit mass defined on an arbitrary region $\mathrm{R} \subseteq \mathrm{B}$ during deformation and $\mathbf{t}(\mathbf{n})$ the surface force per unit area of the boundary $\partial\mathrm{R}$ of R, where $\mathbf{n}$ is the unit outward normal to $\partial\mathrm{R}$. For $\mathbf{t}$ the terminology *traction vector* is often used: it is given by

$$\mathbf{t}(\mathbf{n}) = \boldsymbol{\sigma}^{\mathrm{T}}\mathbf{n}, \tag{8}$$

at each point of $\partial\mathrm{R}$ in terms of the second-order tensor $\boldsymbol{\sigma}$, known as the *Cauchy stress tensor*, which (by Cauchy's theorem) does not depend on $\mathbf{n}$. The associated traction per unit reference area of $\partial\mathrm{R}_\mathrm{r}$ is $\mathbf{S}^{\mathrm{T}}\mathbf{N}$, where $\mathbf{S}^{\mathrm{T}} = J\boldsymbol{\sigma}\mathbf{F}^{-\mathrm{T}}$ is the *first Piola–Kirchhoff stress tensor*. Its transpose $\mathbf{S}$ is known as the *nominal stress tensor*, while $\mathbf{N}$ is the outward unit normal to $\partial\mathrm{R}_\mathrm{r}$.

When there is no inertia contribution, the local *equilibrium equation* may be written in either of the forms

$$\mathrm{div}\,\boldsymbol{\sigma} + \rho\mathbf{b} = \mathbf{0}, \quad \mathrm{Div}\,\mathbf{S} + \rho_\mathrm{r}\mathbf{b} = \mathbf{0}, \tag{9}$$

the Eulerian and Lagrangian forms, with ρ and ρ_r the associated mass densities in B and B_r, respectively. The latter are connected by $\rho_\mathrm{r} = J\rho$. The divergence operators div and Div relate to $\mathbf{x}$ and $\mathbf{X}$, respectively.

Balance of angular momentum requires that $\boldsymbol{\sigma}$ be symmetric when there are no couple stresses present. Thus, $\boldsymbol{\sigma}^{\mathrm{T}} = \boldsymbol{\sigma}, \mathbf{F}\mathbf{S} = \mathbf{S}^{\mathrm{T}}\mathbf{F}^{\mathrm{T}}$.

2.3. Hyperelasticity

An elastic solid that is characterized in terms of a scalar potential function (a so-called strain–energy function) is referred to as a *hyperelastic material*. Then, W, per unit volume in B_r, is dependent on $\mathbf{F}$, i.e. $W(\mathbf{F})$. For an inhomogeneous material, W depends separately on $\mathbf{X}$. Based on W, the formulas for $\mathbf{S}$ and $\boldsymbol{\sigma}$ are

$$\mathbf{S} = \frac{\partial W}{\partial \mathbf{F}}, \quad \boldsymbol{\sigma} = J^{-1}\mathbf{F}\frac{\partial W}{\partial \mathbf{F}}. \tag{10}$$

When evaluated in B_r, where $\mathbf{F} = \mathbf{I}$, the identity tensor, it is usual to measure W from that configuration, so that

$$W(\mathbf{I}) = 0, \quad \frac{\partial W}{\partial \mathbf{F}}(\mathbf{I}) = \boldsymbol{\tau}, \tag{11}$$

it being assumed, for the sake of generality that there is a residual stress $\boldsymbol{\tau}$ resident in B_r. The formulas in (10) are replaced by

$$\mathbf{S} = \frac{\partial W}{\partial \mathbf{F}} - p\mathbf{F}^{-1}, \quad \boldsymbol{\sigma} = \mathbf{F}\frac{\partial W}{\partial \mathbf{F}} - p\mathbf{I}, \tag{12}$$

in the case of an incompressible material, the constraint $J = 1$ requiring the presence of a Lagrange multiplier p. Eq. $(11)_2$ is then replaced by

$$\frac{\partial W}{\partial \mathbf{F}}(\mathbf{I}) - p_\mathrm{r}\mathbf{I} = \boldsymbol{\tau}, \tag{13}$$

in which p_r is the reference configuration value of p.

2.3.1. Objectivity and material symmetry

A basic property of W is that it must be *objective*, i.e. its dependence on $\mathbf{F}$ is not completely arbitrary because it must be independent of superimposed rotations after deformation. This means that, instead of depending on $\mathbf{F}$, which has nine components, it depends only on the $\mathbf{U}$ that appears in the polar decomposition $(6)_1$. By symmetry, this has only six components. Thus, $W = W(\mathbf{U})$, and since $\mathbf{U}^2 = \mathbf{C}$ from $(4)_1$ and $(6)_1$, W may equally well be regarded as a function of $\mathbf{C}$. This independence of $\mathbf{R}$ constitutes the *principle of objectivity*. Henceforth, we sometimes take $\mathbf{C}$ as the independent deformation variable within W, which is then automatically objective.

Other restrictions apply in the presence of material symmetry in B_r. For example, a material for which W is unaffected by *any* rotation in B_r before deformation is said to be *isotropic* relative to B_r, i.e. the material has isotropic symmetry. Then, the restriction $W(\mathbf{Q}^{\mathrm{T}}\mathbf{C}\mathbf{Q}) = W(\mathbf{C})$ is required for any $\mathbf{C}$ and for all rotations $\mathbf{Q}$, which states that W is an isotropic function of $\mathbf{C}$. It follows that W is expressible as a function of just three (in three dimensions) independent invariants of $\mathbf{C}$. These are typically taken to be

$$I_1(\mathbf{C}) = \mathrm{tr}\,\mathbf{C}, \quad I_2(\mathbf{C}) = \frac{1}{2}[I_1(\mathbf{C})^2 - \mathrm{tr}\,(\mathbf{C}^2)], \quad I_3(\mathbf{C}) = \det\mathbf{C}, \tag{14}$$

namely the so-called *principal invariants* of $\mathbf{C}$.

Next, we consider an isotropic material with an embedded preferred direction corresponding to a unit vector $\mathbf{M}$ in B_r, which in general depends on $\mathbf{X}$. Such a material is *transversely isotropic*. Then W depends on the (so-called structure) tensor $\mathbf{M}\otimes\mathbf{M}$ as well as on $\mathbf{C}$. These define the additional invariants

$$I_4(\mathbf{C}) = (\mathbf{C}\mathbf{M})\cdot\mathbf{M}, \quad I_5(\mathbf{C}) = (\mathbf{C}^2\mathbf{M})\cdot\mathbf{M}. \tag{15}$$

For greater generality, we now allow W to depend on the list of invariants $I_1, I_2, \ldots, I_N$ for $N \geq 2$. These depend on $\mathbf{C}$ as well as structure tensors such as $\mathbf{M}\otimes\mathbf{M}$. Then, we use the notation $W = \bar{W}(I_1, I_2, \ldots, I_N)$. By differentiating W with respect to $\mathbf{F}$ for a compressible material the tensors $\mathbf{S}$ and $\boldsymbol{\sigma}$ develop as

$$\mathbf{S} = \sum_{i=1}^{N}\bar{W}_i\frac{\partial I_i}{\partial \mathbf{F}}, \quad \boldsymbol{\sigma} = J^{-1}\mathbf{F}\sum_{i=1}^{N}\bar{W}_i\frac{\partial I_i}{\partial \mathbf{F}}, \tag{16}$$

where we have adopted the shorthand notation $\bar{W}_i = \partial\bar{W}/\partial I_i$, $i = 1, 2, \ldots, N$. The derivatives $\partial I_i/\partial\mathbf{F}$ depend on the kinematics and the structure tensors, while $\bar{W}_i$ characterize the material properties, which depend on the specific form of W.

For an incompressible material, I_3 does not appear in the list of invariants while the formulas (16) are supplemented by a Lagrange multiplier term as in (12). For more detailed discussion of invariants see the excellent article [3].

2.3.2. Fiber-reinforced materials

We now apply the above theory to soft biological tissues, many of which are considered to be incompressible (as assumed henceforth). They are also examples of fiber-reinforced materials, and fiber reinforcement has a key role in identifying their mechanical response. They typically consist of at least two distinct arrangements of collagen fibers. Here we focus on materials consisting of two families of fibers with their local directions in B_r identified by the unit vectors $\mathbf{M}$ and $\mathbf{M}'$.

Then, as well as the invariants I_1, I_2, I_4, I_5 associated with $\mathbf{M}$ for a transversely isotropic material, there are similar invariants, say I_6 and I_7, based on $\mathbf{M}'$. A further invariant I_8 provides a connection between the two fiber families. The additional invariants are given by

$$I_6 = (\mathbf{C}\mathbf{M}')\cdot\mathbf{M}', \quad I_7 = (\mathbf{C}^2\mathbf{M}')\cdot\mathbf{M}', \quad I_8 = (\mathbf{M}\cdot\mathbf{M}')\left[(\mathbf{C}\mathbf{M})\cdot\mathbf{M}'\right]. \tag{17}$$

For an incompressible material W then depends on the seven remaining independent invariants, so that $W = \bar{W}(I_1, I_2, I_4, I_5, I_6, I_7, I_8)$. The values of these invariants in B_r are $I_1 = I_2 = 3$, $I_4 = I_5 = I_6 = I_7 = 1$, $I_8 = \mathbf{M}\cdot\mathbf{M}'$.

Thus, $\boldsymbol{\sigma}$ has the expanded form

$$\begin{aligned}\boldsymbol{\sigma} = &-p\mathbf{I} + 2\bar{W}_1\mathbf{B} + 2\bar{W}_2(I_1\mathbf{B} - \mathbf{B}^2) + 2\bar{W}_4\mathbf{m}\otimes\mathbf{m} + 2\bar{W}_5(\mathbf{m}\otimes\mathbf{B}\mathbf{m} + \mathbf{B}\mathbf{m}\otimes\mathbf{m})\\ &+ 2\bar{W}_6\mathbf{m}'\otimes\mathbf{m}' + 2\bar{W}_7(\mathbf{m}'\otimes\mathbf{B}\mathbf{m}' + \mathbf{B}\mathbf{m}'\otimes\mathbf{m}') + \bar{W}_8(\mathbf{m}\otimes\mathbf{m}' + \mathbf{m}'\otimes\mathbf{m})\mathbf{M}\cdot\mathbf{M}',\end{aligned}$$

wherein $\bar{W}_i = \partial\bar{W}/\partial I_i$ for $i = \in \{1, 2, 4, \ldots, 8\}$, while $\mathbf{m}$ and $\mathbf{m}'$ are the push forwards $\mathbf{F}\mathbf{M}$ and $\mathbf{F}\mathbf{M}'$, respectively. If the reference configuration is free of stress, the conditions

$$2\bar{W}_1 + 4\bar{W}_2 - p_0, \quad \bar{W}_4 + 2\bar{W}_5 = 0, \quad \bar{W}_6 + 2\bar{W}_7 = 0, \quad \bar{W}_8 = 0 \tag{18}$$

must be satisfied there, p_0 being the value of the Lagrange multiplier p therein.

When there are two fiber families the mechanical response of the material is orthotropic if either (a) the fibers are orthogonal in B_r or

(b) the mechanical properties of the two fiber families coincide, which may include the case when they are orthogonal. In case (a) $I_8 = 0$ and W_8 does not then appear in the above expression for $\boldsymbol{\sigma}$.

It is often appropriate, and common practice in characterizing the mechanical response of soft biological tissues, to take W to have the decoupled form

$$W = \bar{W}_{\rm iso}(I_1) + \bar{W}_{\rm fib}(I_4, I_6), \tag{19}$$

where $\bar{W}_{\rm iso}(I_1)$ represents the isotropic properties of the matrix material in which the two families of fibers are embedded and $\bar{W}_{\rm fib}(I_4, I_6)$ represents the anisotropic properties of the fibers themselves. In particular, $\bar{W}_{\rm iso}(I_1)$ is commonly considered to have the neo-Hookean form and $\bar{W}_{\rm fib}(I_4, I_6)$ the Fung-type exponential form, so that

$$\begin{aligned} \bar{W}_{\rm iso}(I_1) &= \frac{1}{2}\mu(I_1 - 3), \\ \bar{W}_{\rm fib}(I_4, I_6) &= \frac{k_1}{2k_2}\{\exp[k_2(I_4 - 1)^2] - 1\} + \frac{k_1}{2k_2}\{\exp[k_2(I_6 - 1)^2] - 1\} \end{aligned} \tag{20}$$

where μ is the shear modulus of the matrix material, while k_1 (with dimension of stress) and k_2 (dimensionless) are material constants associated with fibers (the same for each family). This model was introduced in [4] and has been extended to allow for the dispersion of collagen fibers simply by replacing I_4 and I_6 by their generalized counterparts I_4^* and I_6^* involving a dispersion parameter $\kappa \in [0, 1/3]$ and defined by

$$I_4^* = \kappa I_1 + (1 - 3\kappa) I_4, \quad I_6^* = \kappa I_1 + (1 - 3\kappa) I_6, \tag{21}$$

as developed in [5]. A further generalization to the case in which there is a non-symmetric dispersion has been provided in [6], and a recent review of these and other dispersion models is contained in [7].

Residual stress. Residual stresses are in general present in the unloaded configuration of a soft biological tissue and they make the mechanical response more complicated than in their absence. More sophisticated modeling is therefore required to account for their effects on the mechanical response. This is especially important in respect of tissues such as arteries [2].

Let $\boldsymbol{\tau}$, which is symmetric, denote a typical residual stress in the configuration $\mathrm{B_r}$. By definition [8,9], $\boldsymbol{\tau}$ is in equilibrium, thus satisfying $\mathrm{Div}\,\boldsymbol{\tau} = \mathbf{0}$ in $\mathrm{B_r}$ (body forces omitted) and zero traction on $\partial\mathrm{B_r}$, i.e. $\boldsymbol{\tau}\mathbf{N} = \mathbf{0}$ thereon. It is important to note, however, that $\boldsymbol{\tau}$ depends on $\mathbf{X}$ in $\mathrm{B_r}$ and therefore cannot be uniform.

A residually-stressed solid has elastic properties expressed in terms of a strain–energy function W that depends on both $\mathbf{C}$ and $\boldsymbol{\tau}$, i.e. $W = W(\mathbf{C}, \boldsymbol{\tau})$. For the development of the associated theory we refer to [10], for example.

Inelasticity. Although not the focus of this section, it should be mentioned here that viscoelastic, growth and remodeling behavior should in general be accounted for in the response of soft biological tissues. In particular, as far as viscoelasticity is concerned we draw attention to the concept of fractional derivatives developed in [11] for soft tissues, while for a review of various aspects of growth and remodeling we refer to [12]. See also the extensive account of the theory of growth in the volume [13].

Towards computation. Numerical methods, and most importantly finite element methods, are needed to tackle the formulation of problems with realistic complex geometries. For the implementation of such methods incompressible soft biological tissues are considered to be slightly compressible so as to overcome numerical issues generated by incompressibility. This is facilitated by multiplicatively decoupling $\mathbf{F}$ into a volumetric part and an isochoric part, the latter denoted $\bar{\mathbf{F}}$, so that $\bar{\mathbf{F}} = J^{-1/3}\mathbf{F}$, and hence $\det\bar{\mathbf{F}} = 1$; see, for example,[14,15].

Let $\bar{\mathbf{C}}$ be the corresponding isochoric part of $\mathbf{C}$, i.e. $\bar{\mathbf{F}}^{\rm T}\bar{\mathbf{F}}$. We can then treat W as depending on $\bar{\mathbf{C}}$ and J separately (and residual stress if present). The Cauchy stress can the be written in the decoupled form

$$\boldsymbol{\sigma} = \bar{\boldsymbol{\sigma}} + \frac{\partial W}{\partial J}\mathbf{I}, \quad \text{with} \quad J\bar{\boldsymbol{\sigma}} = 2\bar{\mathbf{F}}\frac{\partial W}{\partial \bar{\mathbf{C}}}\bar{\mathbf{F}}^{\rm T} - \frac{2}{3}\mathrm{tr}\left(\bar{\mathbf{C}}\frac{\partial W}{\partial \bar{\mathbf{C}}}\right)\mathbf{I}, \tag{22}$$

$\bar{\boldsymbol{\sigma}}$ being its deviatoric part. Moreover, $\mathrm{tr}\,\bar{\boldsymbol{\sigma}} = 0$, and $\partial W/\partial J = \mathrm{tr}\,\boldsymbol{\sigma}/3$ is its hydrostatic part. In finite element formulations it is normal to employ the second Piola–Kirchhoff stress tensor, i.e. $J\mathbf{F}^{-1}\boldsymbol{\sigma}\mathbf{F}^{-\rm T}$. See [2] for the relevant background.

The formulation based on (22) is often used in finite element analyses, in particular for soft tissue problems in which W is split into a deviatoric part and a volumetric part (a volumetric–deviatoric split). For an isotropic material, for illustration, this split has the form

$$W(\bar{\mathbf{C}}, J) = W_{\rm iso}(\bar{\mathbf{C}}) + W_{\rm pen}(J), \tag{23}$$

wherein the isochoric and volumetric parts of W are, respectively, $W_{\rm iso}$ and $W_{\rm pen}$. In particular, $W_{\rm pen}$ acts as a penalty term for 'small' $J - 1$ that is used to drive J towards 1.

3. Material testing and data acquisition for constitutive modeling of soft biological tissues

3.1. State-of-the-art

3.1.1. In vitro statically determinate material testing

The most commonly used mechanical test is the uniaxial test on a thin rectangular piece of tissue. The recorded data are the exerted force F along direction $\mathbf{a}$ and the distance between the tensile machine jaws L. The axial stretch and the transverse stretch can also be measured directly through video-extensometer measurements between markers placed on the specimen surface.

According to Saint-Venant's principle, away from the jaws, it can be assumed that the first Piola–Kirchhoff stress tensor is uniform and may be written such as $\mathbf{P} = F/A_0\ \mathbf{a}\otimes\mathbf{a}$, where A_0 is the transverse initial cross section area. If the aspect ratio is roughly below five, ($L/\sqrt{A_0}\ \leq 5$), which may happen when testing brain tissue, parenchyma, or poker-chip shape samples of arteries (radial tension), the Saint-Venant's principle is violated because the deformation and the stress components become inhomogeneous. Multiaxial tests are basically necessary for determining the constitutive parameters of anisotropic soft tissues. Representative multiaxial tests include planar biaxial extension [16], inflation–extension [17] and bulge inflation [18]. For discussion on the limitations of planar biaxial tests for characterizing anisotropic nonlinearly elastic solids, we refer to [19].

In a planar biaxial tensile test, a square sample is simultaneously loaded in two orthogonal directions $\mathbf{a}$ and $\mathbf{b}$. It is usually assumed that the first Piola–Kirchhoff stress tensor is uniform and may be written as $\mathbf{P} = F_a/A_0\ \mathbf{a}\otimes\mathbf{a} + F_b/A_0\ \mathbf{b}\otimes\mathbf{b}$, where F_a and F_b are the exerted forces along directions $\mathbf{a}$ and $\mathbf{b}$ respectively. Although planar biaxial testing offers advantages over uniaxial testing, it is not well suited for strength assessment because hook-based mounting and the square specimen geometry typically prevent failure in the gauge area [20]. Failure analysis is more effectively conducted using bulge inflation tests when they are doable [18]. Note that multiaxial tests are not limited to biaxial tensile conditions, combinations of uniaxial tension and shear, or biaxial tension and shear [21], or even triaxial tension [22], were rarely reported on soft tissues despite the difficulty of ensuring Saint-Venant's conditions in such tests. While many soft tissues are used under tensile conditions in the body, others, like cartilage, have to bear compression loads as in intervertebral discs, e.g., and need to be tested in compression rather than in tension [23].

Eventually, it is worth mentioning that all the previous techniques apply at the tissue scale, where samples of sufficient size (at least 5×5 mm area) are available. For characterizing soft tissue mechanics at a lower scale, microindentation or even nanoindentation, at a single point or in tapping mode, have been used quite intensively [24]. The recorded force versus penetration depth curves can be related to a local

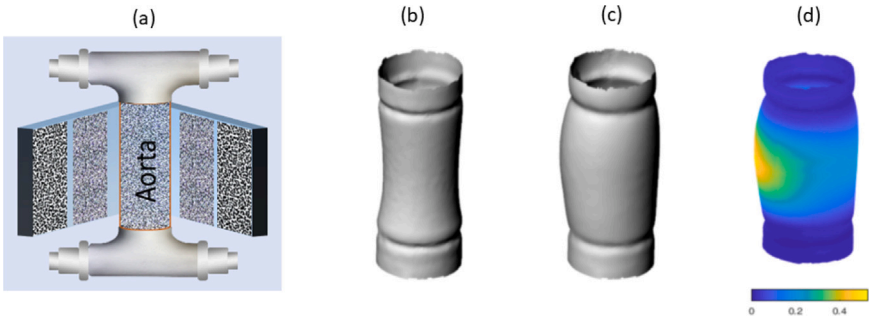

Fig. 1. Schematic of a tension inflation test conducted on a segment of aorta (a) with a multiview camera system. A speckle pattern is painted onto the surface of the aorta and it is imaged with digital cameras directly and indirectly using mirrors. All images are stitched together to reconstruct the undeformed shape (b) and the deformed shape after inflation (c) [29,30]. Digital image correlation is used to process these images and derive local displacement vectors upon inflation. After differentiation, the map of maximum principal logarithmic strain (d) is plotted on the deformed shape [29,30].
Source: Adapted from [30].

indentation stiffness of the tissue, but this approach entails solving very difficult inverse problems when trying to relate the response to constitutive properties of the tissue due to spatial heterogeneities at these scales.

3.1.2. *In vitro statically indeterminate material testing*

Most of the techniques discussed above share the limitation of assuming uniform stress and strain distributions. Statical determination is violated when the aspect ratio is insufficient. The existence of non-uniform material properties provides another source of a statically indeterminate stress field in the central region of the specimens. According to mechanobiology [25], these heterogeneities should be expected as cells need to remodel tissues in order to accommodate local stress variations. Therefore, submillimeter-resolution strain field measurements are needed to characterize the regional variations in tissue mechanical properties.

Digital image correlation (DIC) provides a non-contact means of quantifying complete, full-field surface displacements and strains across diverse material systems [26]. The technique, first introduced by Sutton and collaborators at the University of South Carolina in the early 1980s [27] and subsequently extended to three-dimensional (stereoDIC) configurations [28], has since been widely adopted for 2D and 3D deformation measurements in soft biological tissues at the macroscale.

A key advantage of DIC in soft tissue testing lies in its non-contact character, which reduces the risk of amplifying or altering the intrinsic material response. Moreover, as a full-field technique, DIC enables the identification of local deformation heterogeneities and facilitates their comparison with global average deformations, an important consideration for the study of inhomogeneous materials. DIC can be applied to specimens with diverse surface geometries, whether planar or curved, and is particularly well suited for accurate measurements on cylindrical structures such as blood vessels [29,30], as illustrated in Fig. 1. In addition, it provides point-to-point strain accuracies approaching 0.001 and full-field average accuracies on the order of 50×10^{-6}, enabling comprehensive assessment of both small and large deformations in a single specimen.

3.1.3. *In vivo testing*

Techniques requiring large biopsy samples are clearly impractical, as they cause significant patient discomfort; consequently, *ex vivo* methods are generally limited to very small specimens. In contrast, there is often a need to determine the mechanical properties of soft tissues *in vivo* and *in situ*. Non-invasive *in vivo* skin characterization devices have emerged as promising tools for measurements at the tissue length scale. The functional principles of these devices vary, with the three most commonly employed being suction, indentation, and dynamic shearing [31].

For deeper soft tissues, mechanical characterization typically involves applying a deformation, measuring the resulting displacement field via an imaging technique, and computing the tissue properties by solving an inverse problem—an approach broadly referred to as elastography. The most widely used elastography method, strain elastography (or compression elastography), involves manually deforming the tissue with an ultrasound transducer and inferring tissue stiffness from the observed deformation in the ultrasound images [32]. An extension of this technique, acoustic radiation force impulse (ARFI) elastography [33], employs a focused ultrasound pulse to induce tissue deformation, which is then tracked using rapid ultrasound imaging to generate a qualitative stiffness map. ARFI's primary advantage over strain elastography is its ability to probe tissues beyond those that can be manually compressed, though its depth remains limited by ultrasound penetration.

A common alternative to ultrasound-based elastography is magnetic resonance elastography (MRE), which uses MRI to measure shear wave propagation through soft tissues [34,35]. The shear waves are generated by an MR-compatible mechanical transducer synchronized with image acquisition. Additionally, *in vivo*, non-invasive stimuli can be used to probe tissue mechanics, the most prevalent being the natural pulsatile forces exerted by blood on the arterial wall [36].

3.2. *Recent trends and future directions*

Images of a painted speckle captured with a conventional camera are not always necessary for DIC applications. Alternative imaging modalities, such as optical coherence tomography (OCT), can be employed to achieve micrometer-scale resolution. OCT has advanced rapidly, including the development of real-time acquisition capabilities [38], and enables high-resolution, cross-sectional imaging of tissue microstructure at various sub-surface levels under near-infrared light [39]. The technique has been applied to characterize both soft and hard human tissues, including blood vessels [38], the respiratory tract [40], gastrointestinal tissues [41], and cartilage [42]. Beyond biological tissues, OCT has also been used in biomaterials research, for example in dental materials, porous 3D scaffolds for tissue engineering, and hydrogels [43–46].

OCT can be integrated with mechanical testing devices to characterize the mechanical response of aortic tissues using elastography and other non-contact optical methods [48]. For instance, in [49], stepwise radial tensile tests were performed on descending thoracic aortas from healthy pigs and on ascending thoracic aortic aneurysms in humans, with 3D image volumes (image stacks) acquired from a region of interest after each loading step (Fig. 2). Due to the aorta's complex anisotropic structure and nonlinear mechanical behavior, strain gradients can vary considerably, not only at the surface but also through

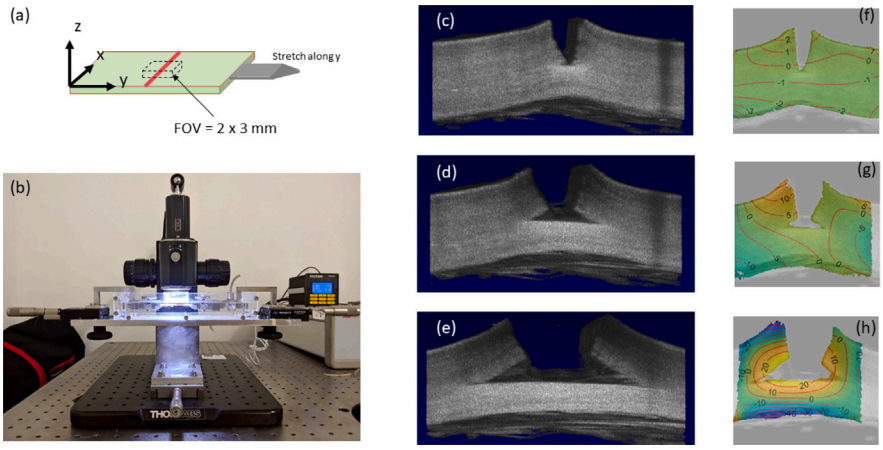

Fig. 2. (a) Experimental overview of quasi-static uniaxial testing of porcine thoracic aorta samples [37]; (b) samples are held at prescribed stretches during optical coherence tomography (OCT) volume acquisition; (c) sequential volumetric OCT images of the porcine thoracic aorta with medial wall defect and under uniaxial tension at 0%; (d) 7%; (e) and 14% average axial strain. Maps of Green Lagrange axial strain E_{xx} measured by digital image correlation (DVC) at (f) 0%;, (g) 7% and (h) 14% average axial strain.
Source: Courtesy of [37].

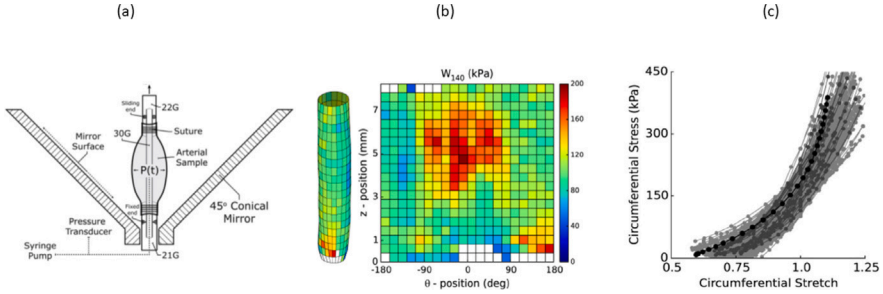

Fig. 3. (a) Schematic overview of a p-DIC system showing the cannulation of a pressure-distended arterial sample at the center of a conical mirror [47]. The gauge needles, with fixed and sliding ends, enables to pressurize and axially stretch the specimen. Spatial distribution of strain energy across an arterial sample; (b) the strain energy density was computed using identified material properties with the virtual fields method [47]. The results are shown for a loaded configurations at $P = 140$ mmHg; (c) reconstructed circumferential stress–stretch behaviors for the same sample for every patch and comparison with standard biaxial testing results (black circles).
Source: Courtesy of [47].

the tissue thickness. In this context, full-field 3D deformation measurements capable of penetrating the tissue are necessary to capture these non-uniformities. Digital volume correlation (DVC) extends beyond the surface-limited information provided by stereoDIC by utilizing volumetric image data, such as 3D stacks composed of multiple 2D cross-sectional images (Fig. 2). Accurate correlation between reconstructed volumes is essential to achieve reliable measurements [50,51], which can be accomplished using local correlation algorithms [51–54].

Other interesting trends related to soft tissue testing are the combination of mechanical tests with microscopic imaging of the tissue structure, as, e.g.:

- Non-invasive imaging of collagen fiber dispersion (multiphoton) in response to mechanical strain [55].
- Negative Poynting effect and its association with collagen cross-links [56,57].
- Time-dependent properties encompassing both the viscoelastic and poroelastic behavior of materials [58,59].
- Frequency-modulated atomic force microscopy [60].
- Multiscale testing with imaging of cells [61] or of fibers [62].
- Multiscale full-field (dense) measurements (Fig. 3).

4. Application to arterial biomechanics

The first subsection on the tissue-specific topic deals with arterial tissue, an important soft tissue of the cardiovascular system. Arterial tissue forms arteries that transport oxygen-rich blood from the heart and regulate blood pressure and blood flow through its (visco)elastic material properties and smooth muscle cells. This subsection provides with a brief overview of the current state of arterial biomechanics and focuses on the microstructure, biomechanical behavior and continuum models for arterials walls using the framework described in Section 2. This subsection concludes with an overview of current trends and future developments in this field and simultaneously leads to Section 7, which deals with machine learning and data mining for soft biological tissues, using vascular tissue as an example.

4.1. State-of-the-art

The passive mechanical behavior of arterial walls is determined by the interplay of elastic fibers, collagen, and the extrafibrillar matrix, while active vascular contractility is governed by the smooth muscle cells (SMCs), which are responsible for maintaining vascular tone and resistance. This has led to constitutive models that can capture tissue properties in both healthy and diseased states. It is generally accepted that the extrafibrillar matrix behaves isotropically [63], while collagen fibers are responsible for tissue anisotropy [4]. Experimental results clearly demonstrate the dispersion of collagen in human arterial layers; collagen is more significantly oriented in the tangential (in-plane) direction than that out-of-plane [64]. However, the collagen fabric

is dependent on vascular topography and (patho)physiological conditions, such as atherosclerosis [65] and abdominal aortic aneurysms, where out-of-plane dispersion is significantly higher than in tissues from healthy samples; for further details see [64]. Typically, each layer of the aged arterial wall, namely, the intima (mechanically insignificant in young and healthy arteries), media, and adventitia, contains two approximately symmetrically arranged fiber families [66]. Collagen fibers in the media are predominantly oriented circumferentially, whereas in the adventitia they are primarily aligned longitudinally [66]. SMCs located in the medial layer also exhibit specific orientations, which may also depend on the (patho)physiological state. These orientations, in turn, depend on the artery type and species, see, e.g., [67] and the references contained therein. Two other primary cell types are present in the arterial walls: fibroblasts produce the structural collagen in the outer layer, while endothelial cells form the internal lining that interfaces with the blood. It is important to note that these three cell types in blood vessels are particularly sensitive to their mechanical stimuli; for further details see, e.g., Humphrey [68].

4.1.1. Microstructure and biomechanical behavior of arterial walls

A healthy but aged elastic artery, which is a large artery near the heart that contains significant amounts of elastic tissue, consists of three main layers: the intima, media and adventitia, as shown in Fig. 4(a). The intima is the innermost layer of blood vessels and is mechanically important, especially with increasing age, as it undergoes thickening with deposition of collagen fibers [69,70]. The media consists of several concentric, interconnected lamellar units, which in mammals have a constant thickness (approximately 15 μm) [71,72], see Fig. 4(a),(c). SMCs are organized into units surrounded by collagen fibers which are embedded the extracellular matrix (ECM) [67], see Fig. 4(c),(d). The medial layer of an artery, the tunica media, handles physiological loads, while the outer layer, the adventitia, acts as a protective, stiff outer sheath to prevent the artery from overstretching under high pressure [4]. Fig. 4(b) shows second harmonic generation images of a healthy (but aged) abdominal aortic wall: at the top an image through-the-thickness is displayed, with the intima on the left (carpet-like collagen structure), followed by a transition layer, and the highly oriented media, followed by another transition layer, and finally the outer tunica adventitia which contains wavy and thicker collagen fiber bundels. Further details can be found in [64].

For better material and computational modeling of arterial tissue, it is crucial to identify the microstructure from the macro-structure to the nano-structure [75] and to identify changes in collagen fiber bundles and elastin fibers in response to physiological loading, e.g., using multi-photon microscopy. Quantifications such as fiber orientation, dispersion, diameter, and waviness are measurable, as recently performed for the adventitia [76] and media [77] of the human abdominal aortas. These parameters must be integrated into computational models, such as those based on representative volume elements (RVEs). A recent review on arterial biomechanics with a focus on microstructural aspects to underpin RVE-based models can be found in [78].

The biomechanical behavior of arterial walls is a combination of passive and active contributions: the passive response is governed by structural components like elastin and collagen, while the active response is a result of SMC contraction. The mechanical response of arterial walls is nonlinear due to the combined effects of collagen and elastin fibers (soft at lower blood pressure, increasingly stiff at higher pressures [79]), anisotropic [80], and viscoelastic [81] (depending on topography), see also [68] for further details. A typical arterial segment contains residual stresses in the unloaded state, best quantified by stretch and curvature [82], and is prestretched *in vivo* depending on age and disease, whereas no axial deformation occurs during a cardiac cycle [83]. In a range of supraphysiological loading, damage-induced softening of the arterial walls occurs [84] and even ruptures can occur, as is the case with aneurysms [85] and dissections [86,87].

SMCs are located in the medial layer of an artery and are crucial for maintaining the artery's mechanical strength and blood pressure through their ability to contract and relax. Smooth muscle contraction/relaxation is regulated by the phosphorylation of myosin light chains, which activates the myosin motors to interact with actin [88]. Activation SMCs causes a decrease in the radial gradient of circumferential stress, until a stable, homeostatic state is reached, i.e. SMC contraction brings the stress closer to a baseline value that is approximately constant across all wall layers and maintains vascular function [89]. In a homeostatic state, which has a stable internal environment within an artery *in vivo*, SMCs that are in a state of partial contraction and form the basal tone of the artery. Changes in the arterial homeostatic state, such as variations in pressure, axial stretch, and flow rate, trigger adaptive responses like growth/atrophy and remodeling [90]. The process of vascular growth and remodeling in response to mechanical and biochemical stimuli, result in hypertrophic SMCs and fragmentation of the internal elastic membrane, increased vessel diameter, and wall thickening. The contraction and relaxation of SMCs lead to a change in lumen diameter, thus regulating resistance to blood flow. The mechanical response to activation is completely different from that after passive loading, which is why studying SMC activation and its effects on arterial function is so important. Fig. 5 illustrates the (nominal) stress–stretch relationship for pig carotid artery medial strips, highlighting a pronounced difference between active and passive mechanical responses.

4.1.2. Constitutive modeling

The arterial wall's mechanical behavior is determined by its microstructure. In particular, the collagen fiber structure and the related dispersion have a dominant impact on the mechanical behavior of vascular walls and must be integrated into a constitutive model [6]. An overview of constitutive arterial models is provided in [91]. One approach that accounts for collagen fiber dispersion is angular integration, first described in [92]. Each fiber is characterized by a strain energy, which is weighted with a normalized angular density of the fibers and subsequently integrated over all orientations. Another approach is based on a structure tensor that accounts for collagen fiber dispersion.

For the angular integration approach, the energy Ψ_f stored in the fiber structure is written as follows

$$\Psi_\mathrm{f} = n \int_S \rho(\mathbf{N}) w(\lambda) \mathrm{d}S, \tag{24}$$

where $\mathbf{N}$ is a unit vector in a general direction in the reference configuration, and w is the stored energy in a collagen fiber with direction $\mathbf{N}$, while λ is the fiber stretch along $\mathbf{N}$. The number of fibers per unit reference volume is n, $\rho(\mathbf{N})$ is the normalized angular density of fibers, and S involves a unit sphere over which the integration is performed. However, several numerical integration methods over S are inaccurate for large deformation problems. Therefore, a discrete fiber dispersion method was introduced, which reduces computational time while maintaining the accuracy of a continuous model [93]. For the structural approach we have

$$\Psi_\mathrm{f} = \hat{\Psi}_\mathrm{f}(\mathbf{C}, \mathbf{H}), \qquad \mathbf{H} = \frac{1}{4\pi} \int_S \rho(\mathbf{N}) \mathbf{N} \otimes \mathbf{N} \mathrm{d}S, \tag{25}$$

where $\mathbf{C}$ is the right Cauchy–Green tensor [2], $\mathbf{H}$ is the deformation-independent generalized structure tensor, and the tensor product is given by $\mathbf{N} \otimes \mathbf{N}$.

A special case of the structure tensor (25), one for each fiber family, was proposed in [6]. The mean fiber direction and two fiber dispersion parameters are characterized by a structure tensor to be fitted with a bivariate von Mises distribution for the orientation density $\rho(\mathbf{N})$. One dispersion parameter describes in-plane dispersion, which quantifies how much the fibers deviate from the primary fiber direction within the tangential plane perpendicular to the radial direction, and out-of-plane dispersion, which quantifies deviation in the radial direction,

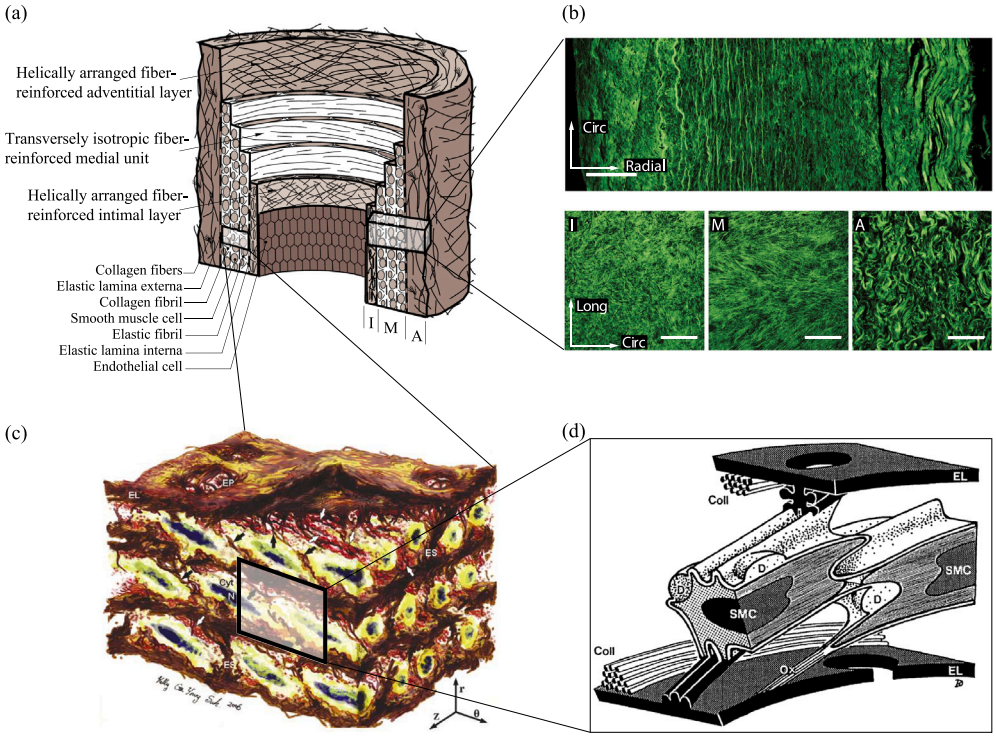

Fig. 4. Histomechanical idealization of a healthy (aged) elastic artery with non-atherosclerotic intimal thickening: (a) wall composed of three layers, i.e. intima – innermost (I), media – middle (M), and adventitia – outermost (A); (b) second harmonic generation images of a healthy (but aged) abdominal aortic wall – on the top an image through-the-thickness is displayed, while the three images on the bottom show in-plane sections of the (I), (M) and (A) (white scale bars corresponding to 100 μm); (c) aortic media's microstructure, highlighting its multi-layered structure of lamellae, smooth muscle cells (SMCs), with elliptical nuclei (N) embedded between elastic lamellas (EL) and surrounded by an extensive network of interlamellar elastin fibers (IEFs shown with black arrows), elastin struts (ES) with reinforced elastin pores (EP); (d) schematic of two SMCs and two fenestrated ELs with their connections—collagen fibers (Coll) are tightly connected to ELs, the left SMC is connected to both EL, the right SMC is connected to the lower EL by oxytalan fibers (Ox), and larger deposits (D) of collagen and heparan sulfate proteoglycan indicates that these molecules are actively interacting with the cell membrane.
Source: From [73].

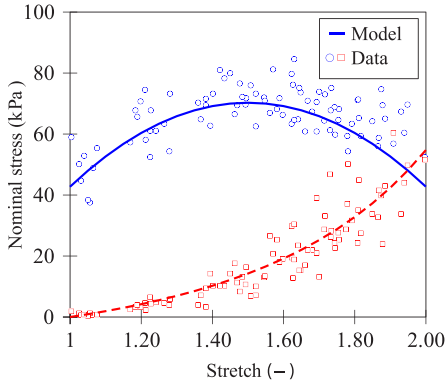

Fig. 5. Relationship between uniaxial nominal stress and stretch for strips of the medial layer of the common carotid artery, differentiating between the active (blue circles) and passive (red squares) mechanical responses, while the curves represent model fits.
Source: From [74].

perpendicular to the artery's surface. The two dispersion parameters capture data of arterial walls with non-symmetric collagen fiber dispersion, as shown, e.g., in [66] based on human non-atherosclerotic thoracic and abdominal aortas, as well as common iliac arteries. However, the related model [6], where, for each set of fiber families, only three structural parameters are needed to model the non-symmetric collagen fiber dispersion and is now widely used to capture the mechanical behavior of a variety of fibrous tissues, including vascular walls, myocardium, heart valves, cornea, adipose tissue, bladder, articular cartilage, and skin, to name a few. The structural approach can also be employed to model the mechanical behavior of diseased tissues such as aneurysmal abdominal aortic tissue [64,94]. This study showed that this collagenous tissue type differs significantly from healthy aortic tissue. In particular, there is a significantly increase of out-of-plane dispersion, leading to variations in material and structural parameters. Interestingly, in abdominal aortic aneurysms, collagen fibers in the abluminal layer lose their waviness and form thicker, straighter struts. Note that both modeling approaches exhibit very similar predictive capabilities for a considerable range of large deformations [95], although they involve different constitutive frameworks. A recent review of nonlinear isotropic and anisotropic constitutive models appropriate for the description of the response of soft biological tissue such as (in)elasticity, viscoelasticity, damage and poroviscoelasticity can be found in [96].

The modeling of muscle activation is part of current research and still requires significant intensification, particularly with regard to the important biochemomechanical coupling effects. The very first model that can describe muscle activation goes back to Hill [99], who received the Nobel Prize for Physiology. Stålhand et al. [98] were the first to use a material law that includes chemical kinetics of smooth muscles, based on the model of Hai and Murphy [100], in combination with nonlinear continuum mechanics. The relationship between active normalized stress ratio T/T_0 and stretch for different calcium concentrations is depicted in Fig. 6. Here, T_0 denotes the minimum stress value in the maximum activated state. In the maximally activated case, stress depends (almost) linearly on stretch, whereas the stress response in activated muscles is strongly nonlinear. Typically, it is assumed that

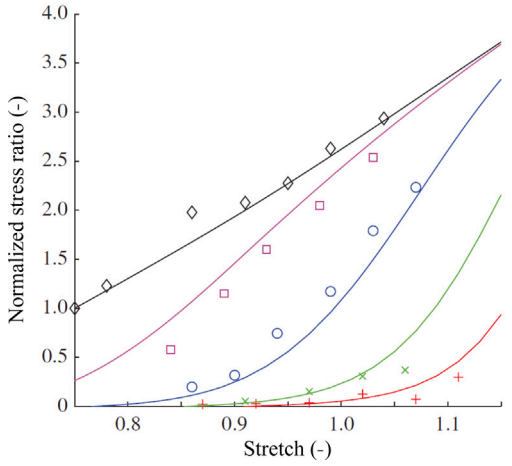

Fig. 6. Relation between normalized stress ratio T/T_0 and stretch for different Ca^{2+} concentrations ($[Ca^{2+}]$), where T_0 denotes the minimum stress value in the maximally activated state (see [97] for data). Black diamonds: $[Ca^{2+}] = 10\,\mu M$; pink squares: $[Ca^{2+}] = 8.9\,\mu M$; blue circles: $[Ca^{2+}] = 4.3\,\mu M$; green crosses: $[Ca^{2+}] = 2.7\,\mu M$; red plus signs: $[Ca^{2+}] = 1.9\,\mu M$; The solid curves correspond to the model results.
Source: From [98].

the total stress σ can be written in the decoupled form $\sigma_p + \sigma_a$, where σ_p is the passive contribution and σ_a is the active contribution. A new multiscale constitutive model that considers arterial contractility at the molecular, cellular, and tissue levels was proposed in [101]. Recent studies on constitutive modeling of vascular smooth muscle cell contraction can be found in [102–104], while the studies in [105–107] focus on the biochemomechanics.

4.2. Recent trends and future directions

Although constitutive models for predicting passive arterial behavior are now well established, newer computational frameworks have been proposed for performing fluid–solid–growth simulations. These approaches integrate structural stress analyses, growth and remodeling (G&R) analyses, and computational fluid dynamics, enabling long-term, patient-specific predictions of evolving hemodynamics, vessel wall morphology, tissue composition, and material properties [108, 109].

However, such models are only clinically useful for prognosis if the constitutive parameters of the G&R models can be identified on a patient-specific basis. These parameters, which may vary regionally, govern processes such as ECM protein turnover and its modulation by local strains, stresses, and stiffness. Furthermore, patient-specific constitutive parameters regarding external tissue support and mechanical properties of tissues, along their spatial heterogeneities, including wall thickness and fiber orientations, represent an unsolved problem—so far, corresponding computational analyses are based on several assumptions and not patient-specific data, which raises questions regarding their agreement with *in vivo* conditions. Only with evolutionary constitutive models can accurate long-term predictions of rupture risk be achieved. One promising avenue is the combination of constrained mixture models [110] with machine learning, contingent upon the availability of comprehensive longitudinal data on aneurysm progression from a sufficiently large patient cohort. Establishing this would require a multi-center database containing 4D MRI images, genetic profiles, blood pressure values, and pulse wave velocities.

Among the various processes driving temporal changes in tissue composition and constitutive properties, aging is widely regarded as a major factor in the onset of cardiovascular diseases. While age-related stiffening of arteries is relatively well characterized [111], computational simulation of the underlying mechanisms at smaller scales remains lacking. To achieve this, stress analysis models would need to be coupled with models of vascular mechanotransduction, such as agent-based models [112], which simulate interactions between biological pathways and their mechanical consequences at the tissue scale [113]. The effects of chemical stimulation can also be incorporated via mathematical models of cellular signaling networks. Despite their potential, predictions from such models require validation using omics data.

To date, these models have not been adapted to patient-specific conditions, including local ECM remodeling and the cell phenotypes associated with vascular aging. Mechanobiological interactions between cells and the ECM, which evolve over multiple timescales (minutes to months), must be considered to capture age-specific vascular adaptations to stimuli such as elastin degradation, phenotypic transitions in vascular smooth muscle cells, and inflammation. Furthermore, the interplay between mechanical forces and aging-related effects, including cellular senescence and endothelial dysfunction, remains largely unexplored across relevant length and time scales. Some computational approaches have attempted to perform stress analyses at the level of medial lamellar units or individual cells [114,115], providing a potential pathway for more detailed mechanobiological modeling.

In conclusion, considerable work remains to be done to develop a new generation of micromechanical computational models that incorporate the mechanobiological effects of vascular aging.

5. Applications to cardiac biomechanics and mechanobiology

The second subsection on the tissue-specific topic deals with cardiac tissue. It is a type of striated muscle (myocardium) consisting of individual heart muscle cells (cardiomyocytes) that are interconnected and enveloped by collagen fibers. Cardiac tissue forms the main part of the heart, which is a central component of the cardiovascular system. This subsection also provides a brief overview of the state-of-the-art of research and describes cardiac mechanics at various scales—from the cellular level to the tissue level and up to the entire heart. Finally, some current trends are presented, such as cardiac digital twins, big data, and the use of engineered heart tissues to better understand cardiac mechanics.

5.1. State-of-the-art

Our understanding of the biomechanics of myocardium has evolved substantially, from initial studies considering the mechanics of the heart using the Law of Laplace [116] to the modern approaches using patient-specific modeling [117–120]. Biomechanical models of the heart have evolved from simplified ellipsoidal left ventricular models [121,122] to incorporate greater anatomical realism, using patient-specific imaging data to construct biventricular [123–125] and four chamber heart models [126,127]. Reflecting the multiphysics nature of muscle mechanics, heart models have evolved to include electromechanics [128–130], fluid–structure interaction [131–134], poroelasticity [135–138] as well as in-depth biochemical processes [139].

Fundamental to the functional modeling of heart muscle is our characterization of passive tissue properties. The passive biomechanics of the heart provide the foundation for representing tissue response to load. Many experimental studies have been performed on myocardial tissue [143–148], highlighting its strong nonlinearity and orthotropy. Modeling these effects relies on our inherent understanding of the local microstructure, where muscle fibers bundled into laminar sheets and layered together create local fiber, sheet and sheet normal directions. From these foundations, hyperelastic constitutive formulations have been developed [149–153]. Among the most commonly deployed in computational models are the Guccione [154] (providing a coupled transversely isotropic representation of the heart), Costa [152] (providing a coupled orthrotropic representation), and Holzapfel–Ogden [153]

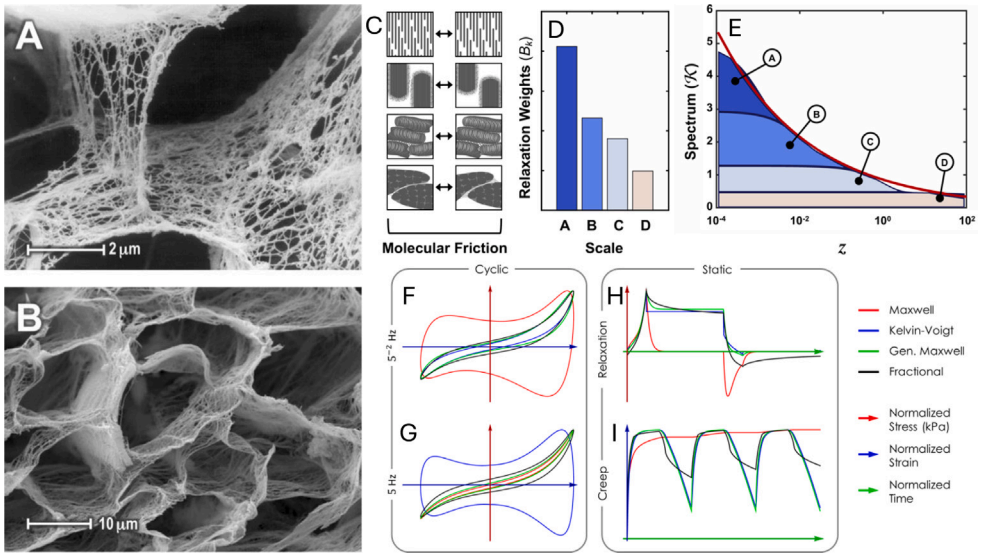

Fig. 7. Scanning electron microscopy of ECM structure in the (A) rabbit and (B) canine myocardium [140]. This results in a (C) multiscale friction processes with a (D) effective density of relaxation phenomena. The spectrum of the multiscale relaxation response is shown in (E), where the colors indicating different scales of response and its representation using a fractional model [141]. The constitutive model of the fractional response is compared against traditional models under (F) high frequency, (G) low frequency, (H) relaxation, and (I) creep testing modalities.
Source: Adapted from [142].

(providing a separated othotropic representation) constitutive relations. These models have been shown to replicate experimental measurements, including uniaxial stretch, biaxial stretch, and triaxial shear. More recently, researchers have developed multimodal experimental protocols integrated with constitutive relations on individual tissue samples specifically optimized to enable unique estimation of material parameters [147].

While the foundation of cardiac mechanical models has focused on hyperelastic formulations, it is well-known experimentally that the heart is, mechanically, a nonlinear poroviscoelastic material (Fig. 7). Capturing the anisotropic viscoelasticity of the heart poses challenges in accurately capturing the rate dependent effects. Some of the first models developed for human myocardium extended the Holzapfel–Ogden formulation using spring–dashpot analogues to define rate-dependent constitutive formulations [155]. While capable of describing individual biaxial and shear responses, it was observed that this model approach required independent parameterizations depending on the experimental data. This limitation stems from the complex relaxation phenomena of the heart, which exhibits behavior more consistent with a power-law [141]. More recent constitutive relations were developed, leveraging fractional viscoelasticity to capture these rate dependent effects across experimental protocols [142]. This formulation further introduced a blended approach between coupling and separable stress terms, enabling more accurate recapitulation of biaxial shear experiments [141]. Building into these models accurate characterizations of the porous effects stemming from fluid motion (either from blood or interstitial fluid) has been attempted [136,137,156], but remains an open challenge in the description of cardiac tissue mechanics.

Critical to capturing the active mechanics of myocardium across the cardiac cycle is the integration of active mechanical constitutive relations. With each beat, electrical stimulation of cardiomyocytes induces contraction through cross-bridge cycling [97,157,158]. Some features of active mechanics in muscle are fundamental, including the Frank–Starling mechanism and force-velocity relationship. However, unlike passive mechanics, which evolves on longer time-scales through growth and remodeling processes, active contraction is highly adaptable and strongly dependent on sarcomeric protein isoforms [159–161], regulation of ionic species [162], metabolism [163], pH [164], as well as the intracellular structural organization of the cell [165,166]. This diverse array of factors has led to an array of constitutive modeling approaches to integrate active mechanics. While some models aim for simplicity by fitting active tension to whole-organ data [124,167], others delve into these intracellular processes through the integration of cell models within the biomechanical framework, offering potential insights into excitation–contraction coupling [168–170] and/or the underlying metabolism of the heart [171].

5.2. Cardiac mechanics across scales

Cardiac function essentially relies on coordinated mechanical action across scales that translate the cycling of sarcomeric proteins into the pumping function of the entire organ. The implementation of these processes relies on the hierarchical structure and function of cardiac tissue, with important biomechanical phenomena occurring at each level.

At the cellular level, biomechanics of the cardiomyocyte depend critically on the generation of force through cross-bridge cycling, the passive mechanics of the cell, and the three dimensional anatomy of the cell. Understanding the active contractile forces generated at the cellular level requires synthesis of cardiac excitation, cross-bridge cycling and metabolic pathways [97,171]. Understanding these pathways at the cellular level, in health and disease, is complex, with experimental techniques ranging from the study of isolated cross-bridge proteins [172], skinned muscle preparations [173,174], and carbon fiber cardiomyocyte preparations [175]. Passive mechanical function of the heart, at the cellular level, is dominated by the large protein titin [176], a large spring-like molecule providing viscoelasticity to the cell [177]. In addition, cardiomyocytes are supported by a scaffolding of desmin, actin and microtubules which interconnect key cellular structures [176]. Critically, these structures create highly aligned myofilaments, t-tubles, and intracellular structures that ensure effective mechanical function of the cell. Understanding and modeling the compendium of these features is currently an open area and is

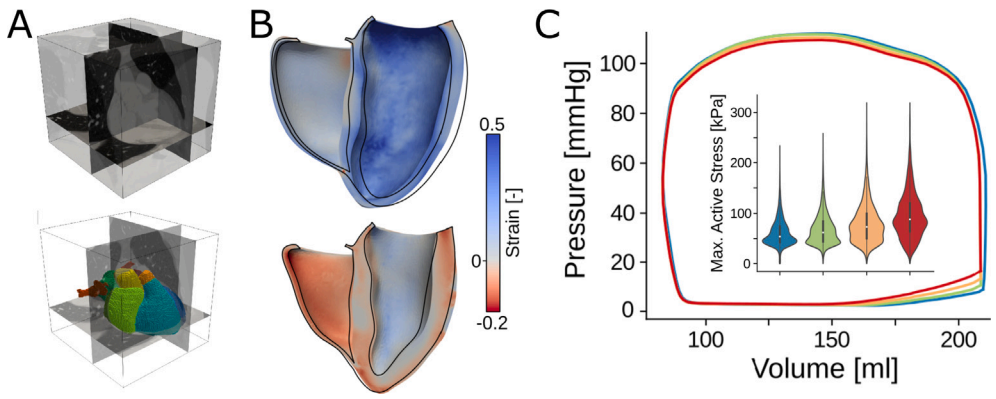

Fig. 8. Personalized digital twins add patient-specific modeling characteristics to capture cardiac behavior over time. (A) 4D CTA with automatic segmentation of the heart chambers and great vessels. (B) Fiber strain in a biventricular heart model. (C) Patient-specific data showing the impact of progressive fibrosis.

key to translating how known variations in disease may impact the biomechanics of the cell.

At the tissue level, cardiac biomechanics extends from individual cardiomyocytes into laminar sheet structures relying critically on the ECM, vasculature, as well as other cell types. Considering cardiomyocytes as the fundamental building blocks of cardiac tissue, these cells are anchored to one another at the intercalated disk (enabling force transmission cell-to-cell) as well as to the ECM at costameres (enabling force transmission cell-to-matrix) [178]. In turn, the ECM provides the key backbone of the tissue, determining the alignment and dispersion of cardiomyocytes and other tissue-level structures through networks of endomysial and perimysial collagen [179]. While much of the mechanics of muscle focus on the cardiomyocyte, the most dominant cell-type of the heart is the endothelial cell [180], reflecting the significant density of the coronary vasculature. Beyond contributing to the mechanics through their arterial walls, coronaries are mechanically loaded structures that dynamically interact with the muscle throughout the heart cycle [136]. Maintaining and adapting this architecture are fibroblasts, which work in concert with cardiomyocytes to respond to changing mechanical demands at the tissue-level. While much of the structure of cardiac tissue is well-known through imaging studies [181, 182], how the mechanics of the fundamental tissue building blocks integrate remains an active area of research [183,184].

At the level of the whole heart, the hierarchy of mechanical effects integrates to drive blood flow. A critical determinant of whole organ mechanics is the fibrous architecture of the myocardial wall, which is most commonly defined through *rule-based* approaches [185–187] but can also be defined from diffusion tensor MRI [188]. Electrophysiological activation of the muscle, trigger contraction, also plays a key role in the biomechanics at the organ-scale, with alterations in conductivity changing the synchronicity of contractions. Interaction blood within the intraventricular chambers drives the preload and afterload experienced by the heart muscle. While often simplified by modeling using pressure boundary conditions, the dependence of tissue mechanics on the blood flow can be significant, particularly in valvular disease. Clinical imaging data, through echocardiography, computed tomography, or MRI, can provide a wealth of data for developing biomechanical models at the whole organ scale. What remains a challenge is the personalization of these biomechanical models, with uncertainties in material characteristics, noninvasive loading conditions (particularly diastolic), determination of the unloaded mechanical state, residual stresses, and external boundary conditions are all thought to play a key role in whole-organ mechanics.

5.3. Recent trends and future directions

Driving the development of cardiac biomechanics are their applications towards understanding disease development, improving diagnosis, and guiding treatment. A key thrust is the development of cardiac digital twins [189–192], which aim to add to personalized patient-specific models of the heart by integrating models that recapitulate the adaptive responses of the heart over time (Fig. 8). This ambitious goal exposes many holes in our current understanding of the heart. Personalization of cardiac models, by determining unknown material characteristics from currently available clinical data remains a challenge. Current approaches often rely on *rules* to combat uncertainty and drive model development, such as creation of rule-based fiber fields [193] or determination of passive mechanics based on the so-called Klotz curve [194]. However, new techniques to grapple with data and improve personalization remain critical. Extending heart models to adaptive digital twins is feasible through growth and remodeling [13, 195–197], with kinematic growth [198] and constrained mixture theory [199] providing a theoretical foundations, as well as detailed biochemical models that describe alterations at the cellular and tissue levels [200,201]. Integration of these adaptive models would enable the prediction of cardiac biomechanics through disease development as well as the potential remodeling and restoration of normative heart function with treatment. Driving these adaptive models on a patient-by-patient level, however, requires personalization of these adaptive mechanisms, which are likely to vary substantively across populations. Beyond the diversity across subjects, the effects of aging within individuals introduces natural long-term dynamics in these adaptive models, changing the adaptivity of the heart throughout life.

Solving the challenges of cardiac digital twins requires integration between biomechanics, data science, and omics. Capturing biomechanical diversity across sex, ethnicity, and age along with disease is increasingly being enabled by large databases, such as UK BioBank [202], FinnGen [203], LifeLines [204], and others. At scale analysis of imaging to heart models [205,206], provides the capacity to capture heart function and potential to personalize cardiac mechanical models. Unlocking the drivers behind observed anatomical, biomechanical, and adaptive diversity in the heart requires integration with other patient data. This includes electronic medical records, potential data from wearable devices, and omics. Linking biomechanics to genomics, transcriptomics, proteomics, and metabolomics is likely to provide key mechanistic insights [207] that can serve to better predict patients' long-term heart function.

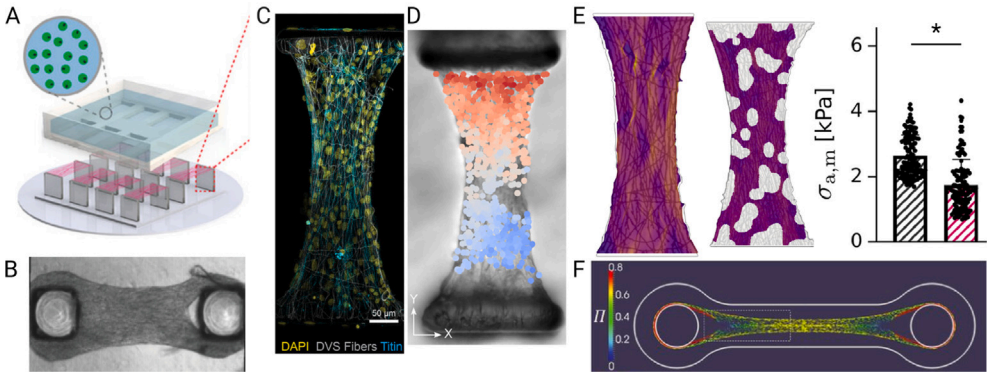

Fig. 9. Use of engineered heart tissues to understand cardiac mechanics. (A) Example of EHT fabrication [178]. (B) Brighfield video of an EHT [62]. (C) Immunofluorescense imaging showing cell nuclei (DAPI), synthetic fibers (DVS fibers) and myofibrils (titin) [62]. (D) Displacement field of a beating EHT obtained using an optical flow analysis [62]. (E) Computational modeling of EHTs grown in different substrate stiffness. Bar plots shows the estimated active stress derived from the model [222]. (F) Simulated stress-driven sarcomeric alignment [220].

With *big data* and biomechanics driving personalized medicine through digital twins at the organ scale, further work towards understanding the keys to mechanics at the tissue and cell level are needed to gain more mechanistic insights into the multiscale nature of cardiac function in health and disease. A promising avenue for investigating these effects is through engineered heart tissues (EHTs), whereby living tissue constructs can be fabricated *in vitro* and studied longitudinally [208–210] (Fig. 9). Developed using induced pluripotent stem cell (iPSC) cardiomyocytes, EHTs can be fabricated at varying scales [211], with platforms providing a mix of cell types [212,213], control of extracellular architecture [178], and integration with disease models [214]. EHT platforms have also been designed to operate at scale [215], providing the capacity to perform large-scale assays examining biochemical or mechanobiological functions in cells and tissues. Modern imaging techniques, like iterative indirect immunofluorescence imaging (4I) [216], enable monitoring of cellular and tissue level protein structures and interactions. Importantly, these EHTs can be mechanically manipulated using stretch protocols [217], electrical pacing [218], pharmacological agents [178], and damage [219] to signaling and mechanobiological drivers of remodeling at the small scale. Integrating EHTs and modeling is at its early stage, but models have proved useful in a range of ways, from elucidating mechanistic drivers of cellular response to stress [220,221] to providing context to experimental results [222]. Continued development of cardiac biomechanics and tissue engineered myocardium promises to significantly improve our basal understanding of fundamental mechanobiological mechanisms of the heart.

6. Applications to brain biomechanics

The final subsection on the tissue-specific topic deals with the very soft, water-rich tissue of the brain, which consists mainly of neurons (for signal transmission throughout the body by means of electrical impulses and neurotransmitters) and glial cells (the essential support system for neurons) organized into gray matter (processing and interpreting information) and white matter (signal transmission). Following a brief review of the biomechanics of the brain at the cell, tissue and organ level, future aspects are highlighted, such as the need to improve multi-field models by considering various coupled processes. Another discussion is on the data-driven discovery of constitutive models, which also leads to the next section.

6.1. State-of-the-art

Traditionally, mechanics is not believed to be a major factor in how the brain works. After all, the brain is nicely isolated from the rest of the world through a hard skull and multiple layers of fluids and tissues. Unlike other major organs, the brain's main function is not to sustain loads, perform mechanical work, or convert external resources to energy. The brain's primary function is to coordinate and regulate bodily activities, processing sensory information to form perceptions, thoughts, and memories. It serves as the central organ of the human nervous system, overseeing both voluntary actions like movement and involuntary ones such as breathing. As such, the brain uses energy provided by the body to organize its homeostatic functions and response to the environment. Hence, the standard approach to neuroscience is to look at the brain as a unit that process information and, essentially, lives outside the physical constraints associated with other organs. Yet, the brain lives in physical space and during both development, life, diseases and trauma the brain strongly depends on mechanical processes. Hence, the influence of mechanics on the brain is of significant interest for developmental and clinical neurobiology [223].

6.1.1. Brain biomechanics at the cell level

At the microscale, mechanical forces affect the behavior of neurons and glial cells in the brain both during development and normal functions as well as during trauma [225]. Indeed, during neural development, mechanical signals play a pivotal role in growth cone navigation, a critical process where the extending processes of neurons find their path to their target destinations to create a functional network that oversees all sensory responses and cognitive tasks. The growth cone is a dynamic motile structure at the tip of each axon [226]. It must interpret multiple information cues from its environment to guide axonal extension [227]. While there has been much emphasis on responses to chemical signals (*chemotaxis*), in recent years it has been found that mechanical cues are also significant. For example, substrate stiffness significantly influences the direction and rate of growth; growth cones typically prefer and extend faster on substrates with intermediate stiffness, an effect known as *durotaxis* [228,229]. Furthermore, the physical topography of the extracellular environment, such as aligned fibers, microgrooves and other axons [230] can also direct axonal growth through contact guidance, where the structural features of the environment mechanically interact with the cytoskeleton of the growth cone (see Fig. 10). This interaction helps steer the growth cone along a physical path that supports the formation of functional neural networks. A multiscale biomechanical model of the interaction of the actin fibers with the cytoplasm, cross-linkers and substrate explains the origin of durotaxis, the response of a growing axon on the substrate stiffness [231].

Once established, these neuronal networks support fast information propagation from multiple neurons through the generation of electrical impulses known as action potentials. When these electrical impulses

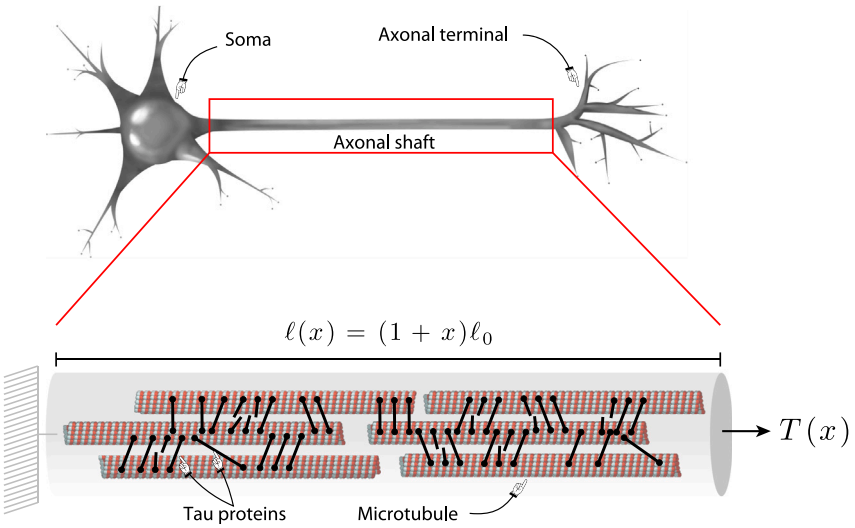

Fig. 10. An essential mechanical structure of the nervous system is the axon, composed internally of microtubules stabilized by tau proteins. Under moderate traction velocities, the axonal core behaves like a viscoelastic Maxwell material.
Source: Adapted from [224].

reach the synapses – the junctions between neurons – they prompt the release of neurotransmitters that cross the synaptic gap and bind to receptors on the postsynaptic neuron, altering its electrical state and potentially triggering a new action potential if the signal is strong enough. Not surprisingly, this delicate process relies also on the proper mechanical environment as it has been shown that synapses without tension fail to fire in hippocampal neurons [232] and that active transport of vesicles in neurons is also modulated by mechanical tension [233]. As a mechanical element, the axon is itself a complicated active solid that inherits its properties from the interaction of internal solid microtubules attached by proteins that bind and unbind, surrounded by a sleeve of contractile viscoelastic actomyosin molecules [224,234,235].

Mechanics at the axonal level also plays a role in any brain trauma that can lead to the rupture axonal connections. In particular, the role of mechanics in nerve regeneration is now well recognized as a critical factor in the repair and regrowth of damaged neural tissues [236]. Mechanical cues, such as substrate stiffness, tension, and the elasticity of the surrounding environment, can significantly influence the behavior of neurons during the regeneration process. For example, optimal stiffness of a scaffold can mimic the natural neural tissue environment, providing support and guidance for growing neurons, enhancing axonal outgrowth and facilitating better alignment and connection with target tissues.

6.1.2. *Brain biomechanics at the tissue level*

The rheology of brain tissue is highly complex due to its ultrasoft, biphasic, and heterogeneous nature. Brain tissue exhibits viscoelastic properties, as its mechanical response depends on both the time and nature of the applied strain. The tissue's high water content (about 80%) further complicates its mechanical behavior, as it can exhibit poroelasticity, where fluid movement within the tissue influences its response to deformation. Testing brain tissue presents significant challenges due to its extreme softness, fragility, and tendency to deform under its own weight.

At the elastic level, brain tissue is considered an ultrasoft material with a low shear modulus, typically on the order of 1 kPa [237], making it much softer than almost all other mature biological tissues (with maybe the exception of adipose tissue [238]). Its elastic behavior is nonlinear and strain stiffening. This nonlinear response is observed across different loading modes, such as uniaxial tension, compression, and shear [239]. Interestingly, brain tissue exhibits an asymmetry in its elastic properties, being stiffer in compression than in tension, likely due to the biphasic nature of the tissue, where cerebrospinal fluid trapped in the matrix provides greater resistance under compression. Additionally, while brain tissue can recover its shape after moderate deformations, excessive strain leads to permanent damage, especially in the fragile axonal fibers.

Several hyperelastic models have been proposed to represent the nonlinear elastic behavior of brain tissue, each capturing different aspects of its strain-stiffening and asymmetric response under tension and compression, including the neo-Hookean model, which using the formalism of Section 2 can be written $W = \mu(I_1 - 3)/2$, where μ is the shear modulus and I_1 is the first invariant of the Cauchy–Green deformation tensor. However, while it has been used for brain tissue, the neo-Hookean model cannot adequately describe its highly nonlinear response at large strains. The next attempt was to use a Mooney–Rivlin model $W = C_1(I_1 - 3) + C_2(I_2 - 3)$, where C_1 and C_2 are material constants, and I_2 is the second invariant of the Cauchy–Green deformation tensor as defined in Section 2. This model captures some degree of nonlinearity but remains insufficient for representing the full complexity of brain tissue behavior [240]. A better approach is to use an Ogden model

$$W = \sum_{i=1}^{n} \frac{2\mu_i}{\alpha_i^2}\left(\lambda_1^{\alpha_i} + \lambda_2^{\alpha_i} + \lambda_3^{\alpha_i} - 3\right), \tag{26}$$

where μ_i and α_i are material parameters. The Ogden model is well suited for brain tissue because it reflects the strain-stiffening behavior and the significant difference between the tension and compression responses [238,241], as shown in Fig. 11.

A radically different approach to constitutive modeling based on machine learning and a data-driven approach was proposed more recently as discussed in detail in Section 7 [242]. This method combines experimental data and computational techniques to automatically discover constitutive models that best describe the mechanical behavior of the material [243,244]. It uses simultaneously different experimental data with different loading modes: uniaxial tension, uniaxial compression, simple shear. These experiments provide data points for the nominal stress as a function of strain in the tissue. Then the method searches within a predefined family of potential models that include different functional forms of the strain–energy function. In particular, for incompressible isotropic material, this family includes terms based on the first invariant I_1 and the second invariant I_2. When applied to the brain, the method finds a rather puzzling result: the best-performing model only depends on the second invariant I_2 [245]. Specifically, the

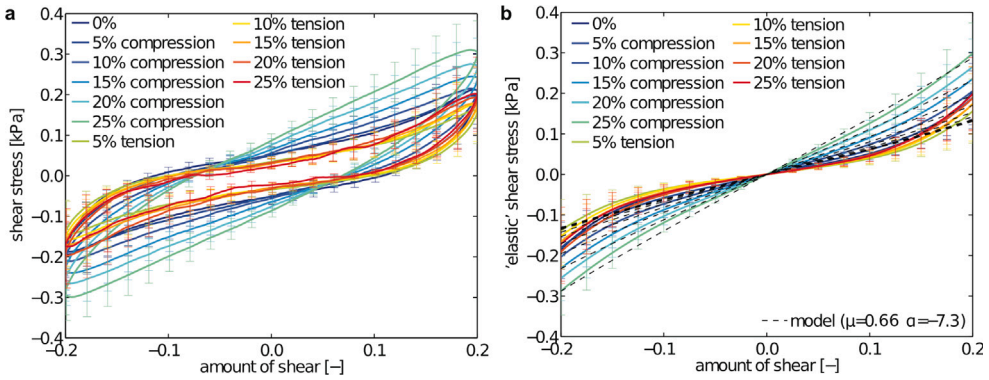

Fig. 11. Modeling compression/tension–shear experiments on brain tissue: (a) mean shear stress as a function of shear deformation; (b) mean "elastic" shear stress against shear deformation, with error bars representing standard deviations, together with the fitted curve from the Ogden strain–energy function (26) using parameters $n = 1, \alpha_1 = -7.3, \mu_1 = 0.66$ (adapted from [239]). The results indicate that an initial compressive strain enhances shear stresses, whereas an initial tensile strain does not.

discovered model that best fits human brain tissue is:

$$W = w_1(I_2 - 3) + w_2\{\exp[w_1(I_2 - 3)] - 1\}, \tag{27}$$

including a linear term $w_1(I_2 - 3)$, which provides a basic linear elastic response and an exponential term $w_2\{\exp[w_1(I_2 - 3)] - 1\}$, which accounts for strain hardening, especially at large deformations.

A model that depends solely on the second invariant I_2 fits brain tissue data effectively due to the unique mechanical properties of the brain's soft tissues, particularly its response to shear deformations. Indeed, in contrast, the first invariant I_1 primarily captures the average stretch and is more relevant for describing isotropic expansions, which are less significant in brain tissue under physiological or pathological conditions. Further, the fact that brain tissue exhibits asymmetry in its stress response to tension and compression suggests that an I_1-based model, which is symmetric in nature, cannot capture these features effectively. However, an I_2-based model inherently incorporates such asymmetries, allowing for more accurate predictions [245]. However, it is important to note that brain tissue typically exhibits a highly hysteretic response during loading and unloading, indicating a significant degree of energy dissipation, which requires visco-elastic and poro-elastic models.

6.1.3. Brain biomechanics at the organ level

At the organ level, mechanics also plays a crucial role in brain function, both in its normal development and in response to trauma. During development, mechanical forces drive processes such as cortical folding and the overall structural organization of the brain [246,247]. Any disruption in these forces can lead to developmental disorders or structural abnormalities. In the context of trauma, external mechanical loads can cause immediate damage to the brain tissue, leading to conditions such as traumatic brain injury (TBI) [248], which may require invasive procedure such as craniectomy to relieve stresses [249].

Starting at the developmental level, the mechanics of brain folding, or gyrification, is a crucial aspect of brain development that allows for the rapid tangential expansion of the cerebral cortex while maintaining a compact volume [250,251]. Several hypotheses have been proposed to explain the mechanisms driving cortical folding during brain development. An older theory is that the *skull-constraint hypothesis*, suggests that the rigid skull restricts brain growth, forcing the cortex to fold as it expands. However, this has largely been discounted as the skull accommodates brain growth [252]. A popular theory among neuroscientists is the *axonal tension hypothesis*, which posits that tension in axons connecting distant regions of the brain pulls cortical areas together, leading to the formation of gyri. Additionally, patterned growth models propose that localized differences in neuronal proliferation and migration drive the formation of primary folds in consistent regions. However, theory, simulations, and experiments on ferret brains have clearly established that axonal tension cannot be the prime driver of folding [253,254].

The third theory is the *differential tangential growth hypothesis*, which proposes that since the outer layers of the cortex grow more rapidly than the underlying layers, a compressive stress is induced that leads to mechanical buckling and folding. This minimal hypothesis accounts for the basic pattern observed and is sufficient to explain the observed variations of thickness between gyri and sulci [255,256]. The wrinkling instability [257] is now recognized as the main factor for folding, including by David van Essen, the initial promoter of axonal tension theory, who wrote: '*the relatively rapid tangential expansion of the cortex has emerged as a driving factor*' [258], relegating axonal tension as a secondary, but potentially important, factor in shaping finer details of brain geometry, such as white matter organization [259]. Importantly, disruptions in the folding process can lead to developmental abnormalities linked to conditions such as epilepsy, autism, and schizophrenia [260], but the precise effects on folding are difficult to pinpoint exactly due to the complexity of these conditions. Hence, gyrification by itself has not yet been conclusively used as a biomarker [261]. In recent years, there has been a great deal of interest in refining these basic mechanical principles, including brain geometry, the role of curvature as shown in Fig. 12, [262,263], and adding axonal tension as a secondary constraint [264–266].

On the traumatic side, mechanics plays a key role in understanding and mediating swelling induced by trauma. In particular, mechanics dominate brain deformations during craniectomy, a surgical procedure where part of the skull is removed to relieve intracranial pressure (ICP). Craniectomy is often performed in cases of traumatic brain injury, stroke, or other conditions that cause swelling of the brain leading to elevated and dangerous ICP. From a mechanical perspective, the craniectomy significantly alters the load distribution on the brain tissue and skull. Normally, the skull provides a rigid boundary that constrains the brain, maintaining internal pressure balance. When a portion of the skull is removed, the brain can expand outward through the opening, reducing ICP. However, the deformation itself is not without danger as it creates large deformations and mechanical stress on the exposed brain tissue that can be computed as shown in Fig. 13, [267,268]. The mechanical deformation due to the loss of this rigid boundary can lead to strain in the brain's soft tissue, which may contribute to secondary injury if not managed properly. Additionally, without the skull's protection, the brain becomes more vulnerable to external mechanical forces, which necessitates careful post-operative monitoring and, in some cases, further intervention such as cranioplasty, where the removed skull portion is replaced after swelling subsides. Recently detailed models including poro-elasticity and allowing for monitoring have also been proposed [269–271].

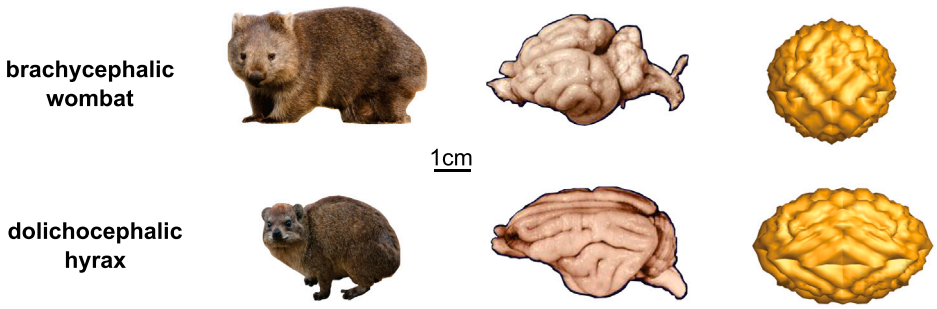

Fig. 12. Mammalian brains exhibit significant differences in shape and degree of gyrification. Simulations of a spheroid with a growing cortical layer and different ellipticities predict transverse folds in brachycephalic skulls and longitudinal folds in dolichocephalic skulls, highlighting the role of substrate curvature in determining fold location.
Source: Adapted from [262].

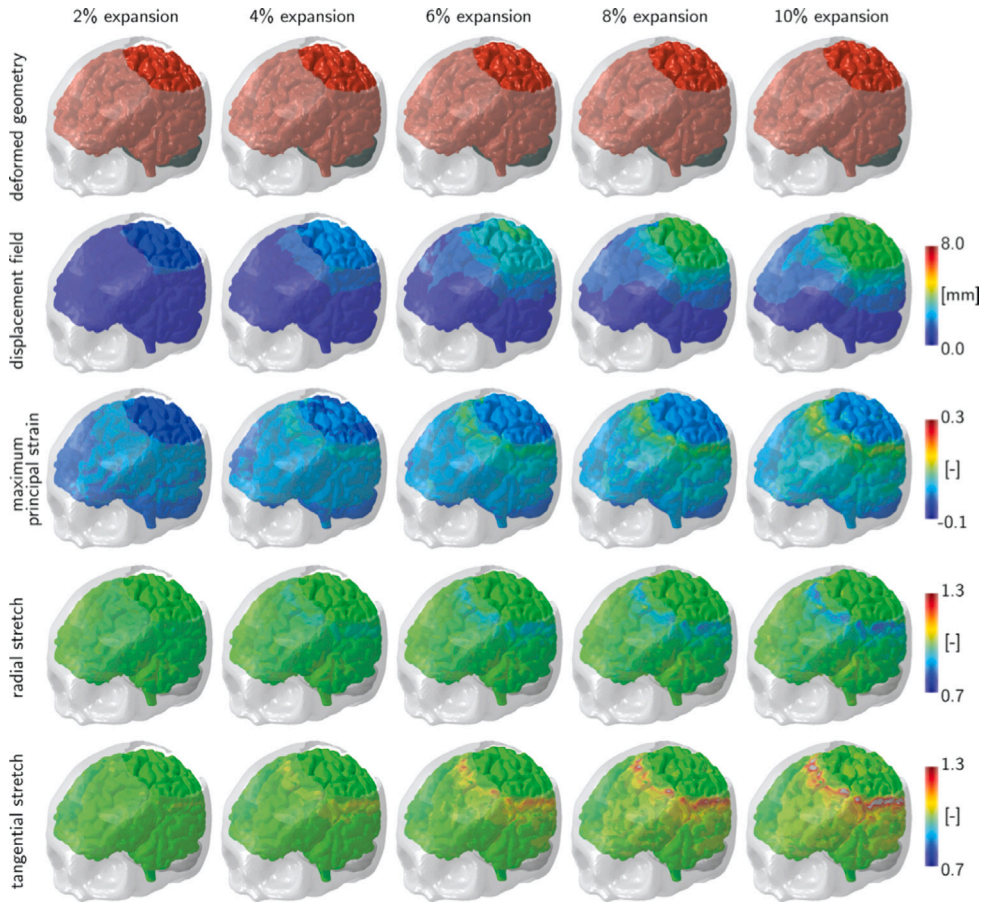

Fig. 13. The temporal evolution of swelling in the left hemisphere is illustrated. Columns correspond to volumetric increases of 2%, 4%, 6%, 8%, and 10% in the white matter of the left hemisphere. The rows present the resulting deformed geometry, displacement, maximum principal strain, radial stretch, and tangential stretch. The highest levels of strain and stretch appear at the margin of the cranial opening, suggesting that axons in this region are particularly vulnerable to mechanical damage and diffuse axonal injury.
Source: From [267].

6.2. Recent trends and future directions

There has been a remarkable increase of interest in brain mechanics in the last 10 years since we first published our call to arms [223].

At the microscopic level, it is now well understood that mechanical forces can modulate cellular processes critical for axonal regeneration, such as by activating mechanosensitive ion channels, influencing gene expression related to growth and repair, and guiding the direction of growth through contact guidance mechanisms [272]. These mechanical aspects are vital not only for the direct manipulation of neuronal growth paths but also for creating an environment conducive to repair, potentially improving outcomes in treatments for spinal cord injuries, peripheral nerve damage, and other neurodegenerative conditions [225]. A combined theoretical, simulation, and experimental approach is now possible with great potential for new treatment.

Another serious gap in the mechanical knowledge of the brain that we identified is the proper characterization of its rheological properties, at the tissue level. The situation has greatly improved with multiple experiments under multiple loadings and under different conditions [273]. These advances together with the remarkable new

data-driven approach to constitutive modeling suggest that we will soon have excellent models for tissue behavior that can be used as a baseline to study several conditions. In particular, it is known that brain stiffness evolves significantly during aging and in the presence of neurological diseases. Studies show that brain tissue tends to soften with age, particularly in conditions such as Alzheimer's disease and multiple sclerosis [274]. Magnetic resonance elastography reveals that the brain's overall elasticity decreases with advancing age, likely due to the degeneration of the ECM and loss of structural integrity in the tissue [273,275,276]. In diseases like multiple sclerosis, demyelination – where the protective myelin sheath around neurons deteriorates – leads to a noticeable reduction in stiffness. Similarly, Alzheimer's disease is associated with a progressive softening of the brain, linked to tau pathology and neuronal loss [277]. These changes in mechanical properties are not uniform throughout the brain, with some regions, such as the cerebellum, showing more pronounced stiffness alterations. Importantly, these stiffness variations can serve as potential biomarkers for early disease diagnosis and tracking disease progression [278].

The data-driven discovery of constitutive models eluded above and discussed in detail in the next section is intrinsically limited by the quality, diversity, and consistency of the underlying experimental data. Sparse datasets, limited loading paths, and experimental noise can bias the inferred strain–energy function towards overly simple or non-physical dependencies, as the learning algorithm is constrained to interpolate rather than genuinely infer underlying mechanisms. However, there are two different approaches. When the functional form of the constitutive model is prescribed *a priori* through a finite combination of candidate terms as proposed in Section 7 where automated discovery is constrained within a predefined model class, then the amount of data required for training is substantially reduced compared to approaches in which the constitutive response is entirely encoded by a neural network. In the first case, the learning task amounts to parameter identification and model selection within a restricted parameter space, which is more robust to limited datasets and benefits directly from embedded physical structure and interpretability. By contrast, fully neural network-based constitutive models involve a high-dimensional parameter space and require large, diverse, and well-conditioned datasets to avoid non-uniqueness and instability. In this setting, data sparsity becomes a critical limitation, as insufficient coverage of strain states can lead to poor generalization and unreliable extrapolation. In the case of brain data, there is not yet sufficient amount of data to train reliably such models. This underscores the importance of model class restriction in regimes where experimental data are scarce.

Yet, it is important to recall that low-quality data increases the risk of over-fitting, lack of identifiability among competing invariants, and spurious model selection, particularly when multiple constitutive forms can explain the data equally well within experimental uncertainty. Regularization, physics-informed constraints, and the explicit enforcement of material symmetries can partially mitigate these issues, but they cannot fully compensate for missing information content in the data. Consequently, results such as the emergence of an I_2-only model for brain tissue should be interpreted with great caution, as they probably reflect limitations of the available experimental protocols rather than a definitive constitutive feature. It is an idealization of the data that would not survive scrutiny if large data sets become available. Yet it gives some insight about how elasticity emerges in such tissues (through surface effects between cells rather than purely entropic effects). For applications, however, one would need to carefully design experiments spanning richer deformation modes and strain regimes to ensure that such data-driven approaches yield robust and physically meaningful constitutive laws, applicable in clinical settings.

At the organ level, the availability of better constitutive models will be crucial to improve simulations for surgical procedures. The problem here is that mechanics is strongly coupled to other physiological processes such as transport of the cerebro-spinal fluid and the electrochemistry of the tissue [279,280]. Hence, there is still a great need to improve multi-field models to take into account multiple coupled processes.

Another interesting recent development at the organ level is the observation that human cortical and subcortical activity can be primarily explained by brain geometry, through the excitations of fundamental brain geometry modes rather than the traditional approach based on inter-regional connectivity [281,282]. Contrary to traditional beliefs, task-evoked activations affect widespread brain modes, challenging the notion of localized brain function. The findings underscore the pivotal role of finer geometric details related to folding in explaining both brain activity [282] and disease [281], suggesting a brand new perspective on brain function based on geometric principles that further reinforces the need to better understand brain folding.

We are therefore right at the cusp of great progress relating geometry and mechanical properties to brain activity and neurological conditions.

7. Machine learning and data mining for constitutive modeling of soft biological tissues

7.1. State-of-the-art

For more than half a century, scientists across the world have made significant strides in testing, modeling, and simulating soft biological tissues, both *ex vivo* and *in vivo* [68,283,284]. For decades, the current gold standard in soft tissue biomechanics has been to first select a constitutive model and then fit its parameters to data [285]. This has resulted in a wide range of competing constitutive models [2], without a clear scientific guidance of which model to choose. Now, machine learning offers powerful tools to simultaneously and fully automatically discover both, the best model and parameters, to describe soft biological tissues [286].

7.1.1. Classical neural networks

Neural networks are a class of models and algorithms that can approximate a wide range of functions [287], independent of any prior knowledge about the data. This versatility not only makes them a powerful tool for classification, reinforcement learning, and generative tasks, but also for regression problems [288], in our case for regression in modeling soft biological tissues [289]. Fig. 14 illustrates a classical neural network with an input layer, two hidden layers with 16 nodes each, and an output layer. The network takes the deformation gradient $\mathbf{F}$ as input and approximates the stress $\boldsymbol{\sigma}$ as output. The hidden layers apply activation functions $f(\circ)$ to the input of each node. The network is fully connected and has a total of 288 parameters or weights $\boldsymbol{\theta} = \{w_i\}$, 16 between the input and the first layer, $w_{0,1}, \dots, w_{0,16}$, 16×16 between the first and second layers $w_{1,1}, \dots, w_{16,16}$, and 16 between the second layer and the output, $w_{1,0}, \dots, w_{16,0}$. During training, the network effectively performs a regression as it learns its parameters by minimizing a loss function L that penalizes the error between model and data. Similarly to the classical nonlinear regression, we can characterize this error as the mean squared error, the L_2-norm [290] of the difference between the predicted stress $\boldsymbol{\sigma}(\mathbf{F}_i, \boldsymbol{\theta})$ and the experimentally measured stress $\hat{\boldsymbol{\sigma}}_i$, divided by the number of data points n, i.e.

$$L(\boldsymbol{\theta}; \mathbf{F}) = \frac{1}{n} \sum_{i=1}^{n} | \boldsymbol{\sigma}(\mathbf{F}_i, \boldsymbol{\theta}) - \hat{\boldsymbol{\sigma}}_i |^2 \rightarrow \min_{\boldsymbol{\theta}}, \tag{28}$$

to learn network weights $\boldsymbol{\theta} = \{w_i\}$. The advantages of neural networks are their universal approximations that let them approximate any continuous function to any degree of accuracy [287], and their inherent flexibility that allows them to model complex nonlinear relations like the constitutive behavior of soft biological tissues [291].

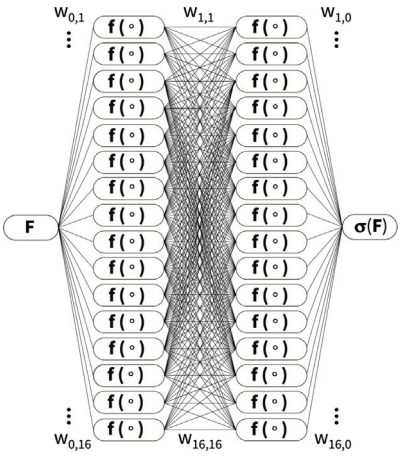

Fig. 14. Classical neural network. Classical neural network with two fully connected hidden layers and 288 weights. The network takes the deformation gradient $\mathbf{F}$ as input and approximates the Cauchy stress $\boldsymbol{\sigma}$ as output. The hidden layers apply activation functions $f(\circ)$ to the input of each node.

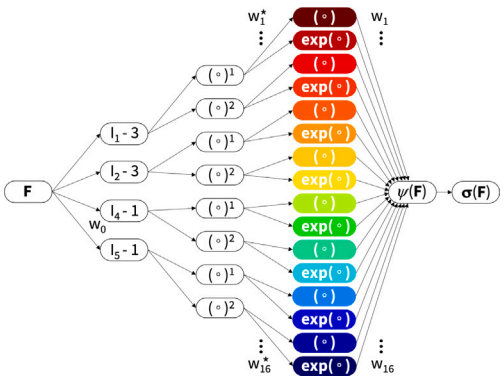

Fig. 15. Constitutive neural network. Constitutive neural network with two sparsely hidden layers and 32 weights. The network takes the deformation gradient $\mathbf{F}$ as input from which it calculates the invariants I_1, I_2, I_4, I_5, and approximates the free-energy function $\psi(I_1, I_2, I_4, I_5)$ from which it calculates the stress $\boldsymbol{\sigma}$ as output. The first layer generates the first and second powers, $(\circ)^1$ and $(\circ)^2$, of the network input and the second layer applies the identity and the exponential, $(\circ)$ and $\exp(\circ)$, to these powers.

Their disadvantages are their computational complexity, especially for densely connected architectures with multiple hidden layers; their risk of overfitting sparse or noisy data; their lack of interpretability; and their inability to generalize well to previously unseen data. Probably most importantly, traditional neural networks cannot and do not include any prior knowledge about the material, their network weights have no physical meaning, and they may violate common physical laws and constraints. This has motivated the question as to how we can best hardwire physical knowledge into the network design?

7.1.2. Constitutive neural networks

Constitutive neural networks represent a distinct class of neural networks that use strain invariants as inputs and produce free-energy functions as outputs. First introduced nearly twenty years ago for modeling rubber-like materials, they have recently regained momentum in the constitutive modeling field [292]. Their use is now expanding within soft tissue biomechanics, with notable applications to skin [293], arterial tissue [294], and the heart [295]. Much like standard neural networks, the early forms of constitutive neural networks relied on multiple hidden layers, conventional activation functions, and hundreds to thousands of adjustable weights [291]. Unsurprisingly, these architectures are highly effective at reproducing complex nonlinear stress–stretch relationships from experimental data in tension, compression, and shear. Yet, one major drawback persists: the difficulty of interpreting the underlying model and its parameters. This challenge raises an important question—can we design constitutive neural networks that not only deliver accurate fits to data, but also provide meaningful insights into the material behavior itself?

7.1.3. Model discovery

The limited interpretability and transferability of conventional neural networks has inspired the development of a new class of constitutive neural networks, designed by reverse-engineering from established constitutive building blocks [286]. These architectures are, by construction, extensions of well-known and broadly accepted constitutive formulations, such as the neo-Hookean [296], Blatz–Ko [297], Mooney–Rivlin [298,299], Demiray [300], Lanir [92], and Holzapfel [4] models. Fig. 15 shows one of these new constitutive neural networks [286]. The network takes the deformation gradient $\mathbf{F}$ as input from which it calculates the invariants I_1, I_2, I_4, I_5, and approximates the free-energy function $\psi(I_1, I_2, I_4, I_5)$ from which it calculates the stress $\boldsymbol{\sigma}$ as output. The first layer generates the first and second powers, $(\circ)^1$ and $(\circ)^2$, of the network input and the second layer applies the identity and the exponential, $(\circ)$ and $\exp(\circ)$, to these powers. The network is sparsely connected and has a total of 32 parameters or weights $\boldsymbol{\theta} = \{w_i\}$, 16 between the first and the second layers, $w_1^*, \dots, w_{16}^*$, and 16 between the second layer and the output, $w_1, \dots, w_{16}$. The constitutive equation of this networks takes the following explicit form,

$$\begin{aligned}\psi = {} & w_1\ w_1^*\ [I_1 - 3] + w_2\ [\exp(w_1^*\ [I_1 - 3]\ ) - 1] \\ & + w_3\ w_3^*\ [I_1 - 3]^2 + w_4\ [\exp(w_4^*\ [I_1 - 3]^2) - 1] \\ & + w_5\ w_5^*\ [I_2 - 3] + w_6\ [\exp(w_6^*\ [I_2 - 3]\ ) - 1] \\ & + w_7\ w_7^*\ [I_2 - 3]^2 + w_8\ [\exp(w_8^*\ [I_2 - 3]^2) - 1] \\ & + w_9\ w_9^*\ [I_4 - 1] + w_{10}\ [\exp(w_{10}^*\ [I_4 - 1]\ ) - 1] \\ & + w_{11}\ w_{11}^*\ [I_4 - 1]^2 + w_{12}\ [\exp(w_{12}^*\ [I_4 - 1]^2) - 1] \\ & + w_{13}\ w_{13}^*\ [I_5 - 1] + w_{14}\ [\exp(w_{14}^*\ [I_5 - 1]\ ) - 1] \\ & + w_{15}\ w_{15}^*\ [I_5 - 1]^2 + w_{16}\ [\exp(w_{16}^*\ [I_5 - 1]^2) - 1].\end{aligned} \tag{29}$$

By design, this free-energy function is a generalization of popular constitutive models where $w_1, \dots, w_{16}^*$ are related to the parameters in the neo-Hookean model [296] associated with the red node, the Demiray model [300] associated with the red nodes, the Blatz-Ko model [297] associated with the orange node, the Mooney Rivlin model [298,299] associated with the dark red and orange nodes, with the Lanir model [92] associated with the dark red and light green nodes, and the Holzapfel model [4] associated with the dark red and turquoise nodes.

Unlike the fully connected classical neural network shown in Fig. 14, the constitutive neural network in Fig. 15 employs a sparse connectivity pattern and contains only 32 trainable parameters or weights $\boldsymbol{\theta} = w_i$—16 linking the two hidden layers and another 16 connecting the second hidden layer to the output. Through minimization of the loss function (28), the network identifies both the most suitable model and the corresponding parameters to capture the mechanics of soft biological tissues. Notably, the weights w_i directly correspond to material parameters, expressed in conventional physical units and carrying a transparent physical meaning [301]. A key challenge that remains, how can we guarantee that the models we discover do not overfit the experiments and generalize well to unseen data?

7.1.4. Sparsity, interpretability, and generalizability

Sparse neural networks adopt an architecture in which many weights are set to zero, thereby limiting the number of active links between adjacent layers. Such sparsity can be introduced post-training through pruning, or enforced during training with dedicated algorithms [289].

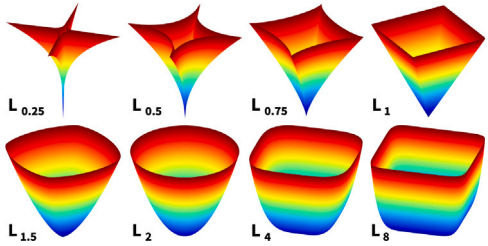

Fig. 16. Inducing sparsity through L_p regularization. Contours of regularization term, $L_p = \alpha \sum_{i=1}^{n_{para}} \|\theta\|_p^p$ with $\|\theta\|_p^p = |w_i|^p$, for varying powers, $p = [0.25, 0.5, 0.75, 1, 1.5, 2, 4, 8]$. For $p \leq 1$, top row, L_p regularization promotes sparsity by setting some weights exactly to zero, but is no longer strictly convex and can have multiple local minima. For $p > 1$, bottom row, L_p regularization promotes stability by reducing outliers, while the regularization term remains convex.
Source: From [289].

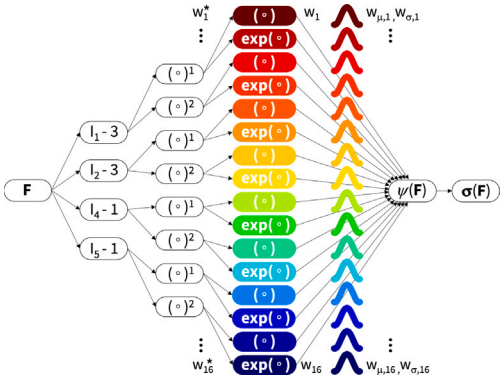

Fig. 17. Bayesian constitutive neural network. Bayesian constitutive neural network with two hidden layers and 64 weights. The network takes the deformation gradient $\mathbf{F}$ as input from which it calculates the invariants I_1, I_2, I_4, I_5, and approximates distributions of the free-energy function $\psi(I_1, I_2, I_4, I_5)$ from which it calculates the stress $\boldsymbol{\sigma}$ as output. Instead of learning point values, the Bayesian network learns means and credible intervals to quantify uncertainty.
Source: From [306].

A common approach to further reduce the parameter space is L_p regularization, also known as bridge regression [302]. First proposed more than thirty years ago, L_p regularization has recently re-emerged as an effective strategy for enforcing sparsity in system identification [303] and, more recently, for data-driven discovery of constitutive models [304]. The method augments the loss function with a penalty term defined by the L_p norm of the parameter vector θ, i.e., the sum of the pth powers of the magnitudes of its $i = 1, \dots, n_{para}$ coefficients w_i, raised to the inverse power, $\|\theta\|^p = [\sum_{i=1}^{n_{para}} |w_i|^p]^{1/p}$ multiplied by a non-negative penalty parameter $\alpha \geq 0$,

$$L(\theta; \mathbf{F}) = \frac{1}{n} \sum_{i=1}^{n} \|\boldsymbol{\sigma}(\mathbf{F}_i, \theta) - \hat{\boldsymbol{\sigma}}_i\|^2 + \alpha \|\theta\|_p^p \rightarrow \min_{\theta}. \tag{30}$$

Fig. 16 illustrates the effects of L_p regularization for varying powers p. Special cases of L_p regularization are L_2 regularization or ridge regression, L_1 regularization or lasso, and L_0 regularization, or discrete subset selection. Among the different approaches, L_1 and L_0 regularization enforce sparsity by driving certain weights exactly to zero, thereby lowering model complexity and enhancing interpretability [290]. The most straightforward technique is L_0 regularization, which transforms continuous model selection into an NP-hard discrete combinatorial task with 2^n possible parameter subsets—rendering it computationally infeasible for large-scale problems. Nevertheless, L_0 regularization remains unique in its ability to explicitly balance interpretability with predictive performance, simplicity with accuracy, and bias with variance [289].

7.1.5. Uncertainty quantification

Uncertainty quantification is critical in the analysis of soft biological tissues to account for variability in biological systems, measurement errors, and model assumptions. It enhances the reliability and accuracy of our predictions, informs decision-making, and ensures the robustness of conclusions, especially in medical applications where personalized modeling is crucial. Bayesian constitutive neural networks are a special type of neural networks that incorporate Bayesian inference to learn uncertainties. They provide a probabilistic interpretation of the network weights and offer uncertainty estimates for our predictions. Fig. 17 illustrates a Bayesian constitutive neural network that builds on our constitutive neural network in Fig. 15 and adds additional weights for uncertainty quantification. During training, the Bayesian network learns means and credible intervals of the network weights using Bayes' theorem [305]. Bayesian neural networks allow us to quantify uncertainty from the probabilistic distributions of the network weights by estimating posterior distributions that capture the inherent variability in the data and in the model parameters. This is particularly important for soft biological tissues that may vary hugely with age, sex, health, and disease.

7.2. Recent trends and future directions

7.2.1. From hyperelasticity to inelasticity

Many soft biological tissues are hyperelastic in their physiological regime, but can become inelastic under non-physiological conditions. This inelasticity can manifest itself in many forms, including viscoelasticity, damage, plasticity, or, most commonly in soft biological tissues, growth and remodeling. Several different approaches are currently emerging to discover inelastic models and parameters from data, including recurrent constitutive neural networks or inelastic constitutive neural networks [307]. Inelastic neural networks are a modular, versatile, and powerful extension of the neural networks in Fig. 15. They not only learn an elastic potential, the free-energy function, but also an inelastic potential, e.g., to characterize tissue growth. While the clinical applications of growth and remodeling are limitless, the success of these methods will depend critically on having sufficient data that characterize the behavior of growing soft tissues non-invasively, longitudinally, at multiple points in time.

7.2.2. From homogeneity to heterogeneity

Especially in view of living soft biological tissues, an important extension of automated model discovery is to generalize the method from homogeneous tension, compression, and shear tests to the analysis of heterogeneous biological systems and statically indeterminate material testing. Unlike traditional approaches that use supervised learning to discover constitutive models from stress–strain pairs, recent studies propose unsupervised learning to discover models from full-field displacement data combined with global force data [308]. A widely used strategy to generate full-field data is digital image correlation, a non-contact optical method that measures full-field displacements and strains on the surface of a sample by analyzing changes in images taken before and after deformation [309]. The clear advantage of this approach is that, in contrast to conventional techniques that need a variety of different tests, full-field methods often only require a single experiment for model discovery [310,311]. This makes it particularly suitable to non-invasively discover models and parameters for biological systems to capture the living material behavior, enhance model precision and reliability, and enable longitudinal studies, for example in the context of growth and remodeling. Full-field methods rely on solving partial differential equations, in our case the balance of linear

momentum. The principle of virtual power can be used through the virtual fields method, where the loss function is built from the deviation between internal and external virtual power [310–314]. Recent trends along these lines involve unsupervised sparse regression in combination with the balance of linear momentum [304] or physics informed neural networks enhanced by symbolic regression [315] and provide promising first results.

7.2.3. From generic to image-based models and personalized simulations

Neural networks and machine learning provide powerful tools for generating geometrical models from medical images by leveraging advanced algorithms for image processing and pattern recognition. Convolutional neural networks can analyze and segment medical images to identify and extract relevant anatomical structures. Generative adversarial networks can then refine these segmented structures to enhance accuracy and resolution. Recent trends suggest training these networks on large datasets of annotated medical images to accurately reconstruct realistic three-dimensional geometries. This allows us to create precise, personalized models with applications in diagnosis, treatment planning, and surgical simulations, towards personalized care and improved patient outcomes.

Patient-specific finite element simulations are advancing as critical tools to integrate the unique anatomical and physiological characteristics of each patient towards personalized assessment and treatment planning. Compared to generic simulations, personalized simulations enhance the accuracy of predicting how soft biological tissues respond to medical interventions and lead to better surgical outcomes and optimized therapeutic strategies. To facilitate the integration of newly discovered models into the finite element workflow without having to implement new user subroutines for every new model, finite element platforms are now beginning to provide user interfaces that directly embed all possible models from the neural network in Fig. 15 into a single universal material subroutine [316,317]. For an application of this approach see [318].

8. Open problems, future directions, and concluding remarks

A great deal has been achieved in the constitutive modeling of soft biological tissues in the last few years, and in this paper we have drawn attention to the current status of the modeling for artery walls, the myocardium and the brain. Much more needs to be done to widen the scope of the modeling to take more detailed account of the microstructure and the different length scales involved, and to account for the interaction of mechanics, biology, chemistry and physics.

Advances in imaging [319,320] will be very important for progressing the modeling along with increasing computer power to solve problems with more realistic geometry and tissue structure. In particular, advances in MRI and computed tomography with different imaging contrasts can lead to consistency between data sets, including geometry, strain and microstructural data, leading to information needed for patient-specific modeling. Imaging results can then be used to refine complex multiscale models over different space, time and energy scales. Constitutive neural networks can be exploited for use in automatic model discovery with related parameters by using experimental data to train the network to optimize constitutive models for a variety of soft tissues, and hence to allow the development of novel treatments for diseases [321].

The combination of imaging results with modeling and simulations at different length scales is important for developing an integrative approach, which will lead to the possibility of exploring the human tissues and organs mechanistically. It is clear that the problems involved are highly complex, and applications of deep learning [322], big data [323], artificial intelligence [324], physics-informed neural networks [325] and constitutive (artificial) neural networks [326,327] will be important for further progress in constitutive and computational modeling, including growth and remodeling [13,328].

It is important to be able to better predict tissue development, adaptation to load changes, responses to injury, implants and surgery, for example. This requires the modeling to build upon available constitutive formulations of the mechanics of tissues to account for temporal changes in particular. Such developments will have an impact on the design of medical devices, surgical interventions, and novel transplant technologies, for example. Validation of computational models *in vivo* is urgently needed, particularly to demonstrate that a parameter-identified model can predict independent, directly measured *in vivo* behavior – especially under controlled perturbations – within quantified uncertainty. This requires techniques that incorporate imaging, physiological measurements, and data at the molecular, cellular, and tissue levels, and ensure that the model accurately predicts biomechanical and mechanobiological complexity.

Moreover, machine learning has the capability to combine the imaging data and multiscale modeling with experimental and clinical data to provide a basis for predictions that improve upon the computational modeling that has been possible up to now [329]. Such modeling will progress the translation of the research results in biomechanics towards clinical practice.

In this paper we have given particular emphasis to the tissues that have attracted significant attention for clinical interventions, specifically the cardiovascular system and the brain. But there is also a need to apply the methods that have been developed to other tissues such as those described in [330]. There is much more work to be done so that full advantage can be taken of the results in clinical practice. For example, computations need to be done fast enough so that they can be used during computer-assisted surgery. Most of the sections have provided a state-of-the-art summary in the area of interest and described related recent trends and future directions. This is a highly interdisciplinary and growing area which is rapidly developing and it offers prospects for the improvement of diagnostics and healthcare. Significantly more funding is required to encourage interdisciplinary interactions and understanding.

CRediT authorship contribution statement

Stéphane Avril: Writing – original draft, Writing – review & editing, Methodology, Conceptualization. **Alain Goriely:** Writing – original draft, Writing – review & editing, Methodology, Conceptualization. **Gerhard A. Holzapfel:** Writing – original draft, Writing – review & editing, Supervision, Methodology, Conceptualization. **Ellen Kuhl:** Writing – original draft, Writing – review & editing, Methodology, Conceptualization. **David Nordsletten:** Writing – original draft, Writing – review & editing, Methodology, Conceptualization. **Ray W. Ogden:** Writing – original draft, Writing – review & editing, Methodology, Conceptualization.

Declaration of competing interest

The authors declare that they have no known competing financial interests or personal relationships that could have appeared to influence the work reported in this paper.

References

[1] R.W. Ogden, Non-linear Elastic Deformations, Dover Publications, New York, 1997.
[2] G.A. Holzapfel, Nonlinear Solid Mechanics. A Continuum Approach for Engineering, John Wiley & Sons, Chichester, 2000.
[3] A.J.M. Spencer, Part III. Theory of invariants, in: A.C. Eringen (Ed.), Continuum Physics, in: volume I – Mathematics, Academic Press, New York, 1971, pp. 239–353.
[4] G.A. Holzapfel, T.C. Gasser, R.W. Ogden, A new constitutive framework for arterial wall mechanics and a comparative study of material models, J. Elasticity 61 (2000) 1–48.
[5] T.C. Gasser, R.W. Ogden, G.A. Holzapfel, Hyperelastic modelling of arterial layers with distributed collagen fibre orientations, J. R. Soc. Interface 3 (2006) 15–35.

[6] G.A. Holzapfel, J.A. Niestrawska, R.W. Ogden, A.J. Reinisch, A.J. Schriefl, Modelling non-symmetric collagen fibre dispersion in arterial walls, J. R. Soc. Interface 12 (2015) 20150188.
[7] G.A. Holzapfel, R.W. Ogden, S. Sherifova, On fibre dispersion modelling of soft biological tissues: a review, Proc. R. Soc. Lond. A 475 (2019) 20180736.
[8] A. Hoger, On the residual stress possible in an elastic body with material symmetry, Arch. Ration. Mech. Anal. 88 (1985) 271–290.
[9] R.W. Ogden, Nonlinear elasticity, anisotropy, material stability and residual stresses in soft tissue, in: G.A. Holzapfel, R.W. Ogden (Eds.), Biomechanics of Soft Tissue in Cardiovascular Systems, in: CISM Courses and Lectures Series 441, Springer, Wien, 2003, pp. 65–108, Section 4.
[10] M. Shams, M. Destrade, R.W. Ogden, Initial stresses in elastic solids: constitutive laws and acoustoelasticity, Wave Motion 48 (2011) 552–567.
[11] W. Zhang, A. Capilnasiu, G. Sommer, G.A. Holzapfel, D.A. Nordsletten, An efficient and accurate method for modeling nonlinear fractional viscoelastic materials, Comput. Methods Appl. Mech. Engrg. 362 (2020) 112834.
[12] D. Ambrosi, M. Ben Amar, C.J. Cyron, A. DeSimone, A. Goriely, J.D. Humphrey, E. Kuhl, Growth and remodelling of living tissues:perspectives, challenges and opportunities, J. R. Soc. Interface 16 (2019) 20190233.
[13] A. Goriely, The Mathematics and Mechanics of Biological Growth, Springer, New York, 2017.
[14] P.J. Flory, Thermodynamic relations for highly elastic materials, Trans. Faraday Soc. 57 (1961) 829–838.
[15] R.W. Ogden, Nearly isochoric elastic deformations: application to rubberlike solids, J. Mech. Phys. Solids 26 (1978) 37–57.
[16] M.S. Sacks, W. Sun, Multiaxial mechanical behavior of biological materials, Annu. Rev. Biomed. Eng. 5 (2003) 251–284.
[17] R. Gleason, S. Gray, E. Wilson, J.D. Humphrey, A multiaxial computer-controlled organ culture and biomechanical device for mouse carotid arteries, J. Biomech. Eng. 126 (2004) 787–795.
[18] A. Romo, P. Badel, A. Duprey, J.-P. Favre, S. Avril, In vitro analysis of localized aneurysm rupture, J. Biomech. 47 (2014) 607–616.
[19] G.A. Holzapfel, R.W. Ogden, On planar biaxial tests for anisotropic nonlinearly elastic solids a continuum mechanical framework, Math. Mech. Solids 14 (2009) 474–489.
[20] J.A. Peña, V. Corral, M.A. Martinez, E. Peña, Over length quantification of the multiaxial mechanical properties of the ascending, descending and abdominal aorta using Digital image correlation, J. Mech. Behav. Biomed. Mater. 77 (2014) 434–445.
[21] S. Dokos, B.H. Smaill, A.A. Young, I.J. LeGrice, Shear properties of passive ventricular myocardium, Am. J. Physiol. Hear. Circ. Physiol. 283 (2002) H2650–H2659.
[22] D.S. Li, R. Avazmohammadi, S.S. Merchant, T. Kawamura, E.W. Hsu, J.H. Gorman 3rd, R.C. Gorman, M.S. Sacks, Insights into the passive mechanical behavior of left ventricular myocardium using a robust constitutive model based on full 3D kinematics, J. Mech. Behav. Biomed. Mater. 103 (2020) 103508.
[23] J.M. Patel, B.C. Wise, E.D. Bonnevie, R.L. Mauck, A systematic review and guide to mechanical testing for articular cartilage tissue engineering, Tissue Eng. Part C Methods 25 (2019) 593–608.
[24] R. Akhtar, M.J. Sherratt, J.K. Cruickshank, B. Derby, Characterizing the elastic properties of tissues, Mater. Today (Kidlington) 14 (2011) 96–105.
[25] J.D. Humphrey, Vascular adaptation and mechanical homeostasis at tissue, cellular, and sub-cellular levels, Cell Biochem. Biophys. 50 (2008) 53–78.
[26] M. Palanca, G. Tozzi, L. Cristofolini, The use of digital image correlation in the biomechanical area: a review, Int. Biomech. 3 (2016) 1–21.
[27] M.A. Sutton, W. Wolters, W. Peters, W. Ranson, S. McNeill, Determination of displacements using an improved digital correlation method, Image Vis. Comput. 1 (1983) 133–139.
[28] H. Schreier, J.-J. Orteu, M.A. Sutton, Image Correlation for Shape, Motion and Deformation Measurements: Basic Concepts, Theory and Applications, Springer Science & Business Media, 2009.
[29] K. Genovese, P. Badel, C. Cavinato, B. Pierrat, M.R. Bersi, S. Avril, J.D. Humphrey, Multi-view digital image correlation systems for in vitro testing of arteries from mice to humans, Exp. Mech. 61 (2021) 1455–1472.
[30] B. Wang, X. Zheng, Y. Zhao, X. Du, H. Ci, S. Avril, Y Tian, L. Li, Y. Mei, Full-field dynamic mechanical characterization of the aorta by 360-degree full-surface mirror-assisted panoramic digital image correlation, Opt. Laser Technol. 192 (2025) 113789.
[31] A. Nava, E. Mazza, M. Furrer, P. Villiger, W.H. Reinhart, In vivo mechanical characterization of human liver, Med. Image Anal. 12 (2008) 203–216.
[32] J. Ophir, S.K. Alam, B.S. Garra, F. Kallel, E.E. Konofagou, T. Krouskop, C.R. B. Merritt, R. Righetti, R. Souchon, S. Srinivasan, T. Varghese, Elastography: Imaging the elastic properties of soft tissues with ultrasound, J. Med. Ultrason. 29 (2002) 155–171.
[33] D. Yildirim, Ö. Akıncı, D.E. Tekcan, Quantitative ultrasound elastography of breast: a review and update with emphasis on shear wave imaging (ARFI), Open J. Med. Imaging 11 (2021) 58–72.
[34] R. Muthupillai, R.L. Ehman, Magnetic resonance elastography, Nat. Med. 2 (1996) 601–603.
[35] S.F. Bensamoun, S.I. Ringleb, L. Littrell, Q. Chen, M. Brennan, R.L. Ehman, K.-N. An, Determination of thigh muscle stiffness using magnetic resonance elastography, J. Magn. Reson. Imaging 23 (2006) 242–247.
[36] S. Avril, J.M. Huntley, R. Cusack, In vivo measurements of blood viscosity and wall stiffness in the carotid using PC-MRI, Eur. J. Comput. Mech. 18 (2009) 9–20.
[37] B. Lane, S. Sherifova, V. Acosta Santamaría, J. Molimard, G.A. Holzapfel, S. Avril, Novel experimental methods to characterize the mechanical properties of the aorta, in: T.C. Gasser, S. Avril, J.A. Elefteriades (Eds.), Biomechanics of the Aorta, Academic Press, 2024, pp. 91–108, Chapter 5.
[38] H. Yabushita, B.E. Bouma, S.L. Houser, H.T. Aretz, I.-K. Jang, K. H Schlendorf, C.R. Kauffman, M. Shishkov, D.-H. Kang, E.F. Halpern, G.J. Tearney, Characterization of human atherosclerosis by optical coherence tomography, Circulation 106 (2002) 1640–1645.
[39] S.A. Boppart, J. Herrmann, C. Pitris, D.L. Stamper, M.E. Brezinski, J.G. Fujimoto, High-resolution optical coherence tomography-guided laser ablation of surgical tissue, J. Surg. Res. 82 (1999) 275–284.
[40] C. Pitris, M.E. Brezinski, B.E. Bouma, G.J. Tearney, J.F. Southern, J.G. Fujimoto, High resolution imaging of the upper respiratory tract with optical coherence tomography: a feasibility study, Am. J. Respir. Crit. Care Med. 157 (1998) 1640–1644.
[41] J.A. Izatt, M.D. Kulkarni, H.-W. Wang, K. Kobayashi, M.V. Sivak, Optical coherence tomography and microscopy in gastrointestinal tissues, IEEE J. Sel. Top. Quantum Electron. 2 (1996) 1017–1028.
[42] J.M. Herrmann, C. Pitris, B.E. Bouma, S.A. Boppart, C.A. Jesser, D.L. Stamper, J.G. Fujimoto, M.E. Brezinski, High resolution imaging of normal and osteoarthritic cartilage with optical coherence tomography, J. Rheumatol. 26 (1999) 627–635.
[43] Y. Yang, P.O. Bagnaninchi, M. Ahearne, R.K. Wang, K.-K. Liu, A novel optical coherence tomography-based micro-indentation technique for mechanical characterization of hydrogels, J. R. Soc. Interface 4 (2007) 1169–1173.
[44] Y.-P. Huang, Y.-P. Zheng, S.-Z. Wang, Z.-P. Chen, Q.-H. Huang, Y.-H. He, An optical coherence tomography (OCT)-based air jet indentation system for measuring the mechanical properties of soft tissues, Meas. Sci. Technol. 20 (2008) 015805.
[45] J.P. Williamson, R.A. McLaughlin, W.J. Noffsinger, A.L. James, V.A. Baker, A. Curatolo, J.J. Armstrong, A. Regli, K.L. Shepherd, G.B. Marks, et al., Elastic properties of the central airways in obstructive lung diseases measured using anatomical optical coherence tomography, Am. J. Respir. Crit. Care Med. 183 (2011) 612–619.
[46] E. Real, A. Eguizabal, A. Pontón, M.C. Díez, J.F. Val-Bernal, M. Mayorga, J.M. Revuelta, J.M. López-Higuera, O.M. Conde, Optical coherence tomography assessment of vessel wall degradation in thoracic aortic aneurysms, J. Biomed. Opt. 18 (2013) 126003.
[47] M.R. Bersi, C. Bellini, P. Di Achille, J.D. Humphrey, K. Genovese, S. Avril, Novel methodology for characterizing regional variations in the material properties of murine aortas, J. Biomech. Eng. 138 (2016) 071005.
[48] J. Rogowska, N. Patel, J.G. Fujimoto, M. Brezinski, Optical coherence tomographic elastography technique for measuring deformation and strain of atherosclerotic tissues, Heart 90 (2004) 556–562.
[49] M. Di Giuseppe, M. Zingales, S. Pasta, S. Avril, In vitro measurement of strain localization preceding dissection of the aortic wall subjected to radial tension, Exp. Mech. 61 (2021) 119–130.
[50] F. Gillard, R. Boardman, M. Mavrogordato, D. Hollis, I. Sinclair, F. Pierron, M. Browne, The application of digital volume correlation (DVC) to study the microstructural behaviour of trabecular bone during compression, J. Mech. Behav. Biomed. Mater. 29 (2014) 480–499.
[51] S.D. Keyes, F. Gillard, N. Soper, M.N. Mavrogordato, I. Sinclair, T. Roose, Mapping soil deformation around plant roots using in vivo 4D X-ray computed tomography and digital volume correlation, J. Biomech. 49 (2016) 1802–1811.
[52] V.A. Acosta Santamaría, M. Flechas García, J. Molimard, S. Avril, Three-dimensional full-field strain measurements across a whole porcine aorta subjected to tensile loading using optical coherence tomography–digital volume correlation, Front. Mech. Eng. 4 (2018) 3.
[53] J. Fu, F. Pierron, P.D. Ruiz, Elastic stiffness characterization using three-dimensional full-field deformation obtained with optical coherence tomography and digital volume correlation, J. Biomed. Opt. 18 (2013) 121512.
[54] L. Liu, E.F. Morgan, Accuracy and precision of digital volume correlation in quantifying displacements and strains in trabecular bone, J. Biomech. 40 (2007) 3516–3520.
[55] C. Cavinato, P. Badel, W. Krasny, S. Avril, C. Morin, Experimental characterization of adventitial collagen fiber kinematics using second-harmonic generation imaging microscopy: similarities and differences across arteries, species and testing conditions, in: Y. Zhang (Ed.), Multi-Scale Extracellular Matrix Mechanics and Mechanobiology, Vol. 23, 2020, pp. 123–164.
[56] M. Destrade, C.O. Horgan, J.G. Murphy, Dominant negative poynting effect for soft tissues, 2020, arXiv preprint arXiv:2009.08750.
[57] S. Teichtmeister, G.A. Holzapfel, A constitutive model for fibrous tissues with cross-linked collagen fibers including dispersion with an analysis of the poynting effect, J. Mech. Phys. Solids 164 (2022) 104911.
[58] H.W. Haslach Jr, J. Gipple, J. Harwerth, J. Rabin, Interstitial fluid–solid interaction within aneurysmal and non-pathological human ascending aortic tissue under translational sinusoidal shear deformation, Acta Biomater. 113 (2020) 452–463.

[59] W. Zhang, J. Jilberto, G. Sommer, M.S. Sacks, G.A. Holzapfel, D.A. Nordsletten, Simulating hyperelasticity and fractional viscoelasticity in the human heart, Comput. Methods Appl. Mech. Engrg. 411 (2023) 116048.
[60] R. Garcia, Nanomechanical mapping of soft materials with the atomic force microscope: methods, theory and applications, Chem. Soc. Rev. 49 (2020) 5850–5884.
[61] T.M. Rothermel, Z. Win, P.W. Alford, Large-deformation strain energy density function for vascular smooth muscle cells, J. Biomech. 111 (2020) 110005.
[62] H. Kobeissi, J. Jilberto, M.C. Karakan, X. Gao, S.J. DePalma, S.L. Das, L. Quach, J. Urquia, B.M. Baker, C.S. Chen, D. Nordsletten, E. Lejeune, MicroBundleCompute: automated segmentation, tracking, and analysis of subdomain deformation in cardiac microbundles, PLoS One 19 (2024) e0298863.
[63] H. Weisbecker, C. Viertler, D.M. Pierce, G.A. Holzapfel, The role of elastin and collagen in the softening behavior of the human thoracic aortic media, J. Biomed. Eng. 46 (2013) 1859–1865.
[64] J.A. Niestrawska, Ch. Viertler, P. Regitnig, T.U. Cohnert, G. Sommer, G.A. Holzapfel, Microstructure and mechanics of healthy and aneurysmatic abdominal aortas: experimental analysis and modeling, J. R. Soc. Interface 13 (2016) 20160620.
[65] S.R. Watson, S.M. Lessner, (Second) harmonic disharmony: nonlinear microscopy shines new light on the pathology of atherosclerosis, Microsc. Microanal. 22 (2016) 589–598.
[66] A.J. Schriefl, G. Zeindlinger, D.M. Pierce, P. Regitnig, G.A. Holzapfel, Determination of the layer-specific distributed collagen fiber orientations in human thoracic and abdominal aortas and common iliac arteries, J. R. Soc. Interface 9 (2012) 1275–1286.
[67] M.K. O'Connell, S. Murthy, S. Phan, C. Xu, J. Buchanan, R. Spilker, R.L. Dalman, C.K. Zarins, W. Denk, C.A. Taylor, The three–dimensional micro– and nanostructure of the aortic medial lamellar unit measured using 3D confocal and electron microscopy imaging, Matrix Biol. 27 (2008) 171–181.
[68] J.D. Humphrey, Cardiovascular Solid Mechanics. Cells, Tissues, and Organs, Springer-Verlag, New York, 2002.
[69] P.B. Canham, H.M. Finlay, J.G. Dixon, D.R. Boughner, A. Chen, Measurements from light and polarised light microscopy of human coronary arteries fixed at distending pressure, Cardiovasc. Res. 23 (1989) 973–982.
[70] G.A. Holzapfel, G. Sommer, C.T. Gasser, P. Regitnig, Determination of layer-specific mechanical properties of human coronary arteries with nonatherosclerotic intimal thickening, and related constitutive modeling, Am. J. Physiol. Hear. Circ. Physiol. 289 (2005) H2048–2058.
[71] H. Wolinsky, S. Glagov, A lamellar unit of aortic medial structure and function in mammals, Circ. Res. 20 (1967) 90–111.
[72] H. Wolinsky, S. Glagov, Comparison of abdominal and thoracic aortic medial structure in mammals, deviation of man from the usual pattern, Circ. Res. 25 (1969) 677–686.
[73] S. Sherifova, G.A. Holzapfel, Biomechanics of aortic wall failure with a focus on dissection and aneurysm: a review, Acta Biomater. 99 (2019) 1–17.
[74] S.C. Murtada, A. Arner, G.A. Holzapfel, Experiments and mechanochemical modeling of smooth muscle contraction: significance of filament overlap, J. Theoret. Biol. 297 (2012) 176–186.
[75] A. Pukaluk, A. Wittgenstein, G. Leitinger, D. Kolb, D. Pernitsch, S.A. Schneider, P. Knöbelreiter, V. Horak, K. Bredies, G.A. Holzapfel, T. Pock, G. Sommer, An ultrastructural 3D reconstruction method for observing the arrangement of collagen fibrils and proteoglycans in the human aortic wall under mechanical load, Acta Biomater. 141 (2022) 300–314.
[76] A. Pukaluk, H. Wolinski, Ch. Viertler, P. Regitnig, G.A. Holzapfel, G. Sommer, Changes in the microstructure of the human aortic adventitia under biaxial loading investigated by multi-photon microscopy, Acta Biomater. 161 (2023) 154–169.
[77] A. Pukaluk, H. Wolinski, Ch. Viertler, P. Regitnig, G.A. Holzapfel, G. Sommer, Changes in the microstructure of the human aortic medial layer under biaxial loading investigated by multi-photon microscopy, Acta Biomater. 151 (2022) 396–413.
[78] M. Dalbosco, E.A. Fancello, G.A. Holzapfel, Multiscale computational modeling of arterial micromechanics: a review, Comput. Methods Appl. Mech. Engrg. 425 (2024) 116916.
[79] M.R. Roach, A.C. Burton, The reason for the shape of the distensibility curves of arteries, Canad. J. Biochem. Physiol. 35 (1957) 681–690.
[80] Y.C. Fung, Elasticity of soft tissues in simple elongation, Am. J. Physiol. 213 (1967) 1532–1544.
[81] F.H. Silver, I. Horvath, D.J. Foran, Viscoelasticity of the vessel wall: the role of collagen and elastic fibers, Crit. Rev. Biomed. Eng. 29 (2001) 279–302.
[82] G.A. Holzapfel, G. Sommer, M. Auer, P. Regitnig, R.W. Ogden, Layer-specific 3D residual deformations of human aortas with non-atherosclerotic intimal thickening, Ann. Biomed. Eng. 35 (2007) 530–545.
[83] C.A.J. Schulze-Bauer, C. Mörth, G.A. Holzapfel, Passive biaxial mechanical response of aged human iliac arteries, J. Biomech. Eng. 125 (2003) 395–406.
[84] G.A. Holzapfel, C.A.J. Schulze-Bauer, M. Stadler, Mechanics of angioplasty: Wall, balloon and stent, in: J. Casey, G. Bao (Eds.), Mechanics in Biology, vol. 46, The American Society of Mechanical Engineers (ASME). New York, AMD-Vol. 242/BED-, 2000, pp. 141–156.
[85] J.D. Humphrey, G.A. Holzapfel, Mechanics, mechanobiology, and modeling of human abdominal aorta and aneurysms, J. Biomech. 45 (2012) 805–814.
[86] K. Bäumler, M. Rolf-Pissarczyk, R. Schussnig, T.-P. Fries, G. Mistelbauer, M.R. Pfaller, A.L. Marsden, D. Fleischmann, G.A. Holzapfel, Assessment of aortic dissection remodeling with patient-specific fluid–structure interaction models, IEEE T. Biomed. Eng. 72 (2025) 953–964.
[87] M. Rolf-Pissarczyk, R. Schussnig, T.-P. Fries, D. Fleischmann, J.A. Elefteriades, J.D. Humphrey, G.A. Holzapfel, Mechanisms of aortic dissection: from pathological changes to experimental and in silico models, Prog. Mater. Sci. 150 (2025) 101363.
[88] S. Murtada, G.A. Holzapfel, Investigating the role of smooth muscle cells in large elastic arteries: a finite element analysis, J. Theoret. Biol. 358 (2014) 1–10.
[89] J.D. Humphrey, Native properties of cardiovascular tissues: Guidlines of functional tissue engineering, in: F. Guilak, D.L. Butler, St.A. Goldstein, D.J. Mooney (Eds.), Functional Tissue Engineering, Springer-Verlag, New York, 2003, pp. 35–45.
[90] Z.S. Jackson, A.I. Gotlieb, B.L. Langille, Wall tissue remodeling regulates longitudinal tension in arteries, Circ. Res. 90 (2002) 918–925.
[91] G.A. Holzapfel, R.W. Ogden, Constitutive modelling of arteries, Proc. R. Soc. Lond. A 466 (2010) 1551–1597.
[92] Y. Lanir, Constitutive equations for fibrous connective tissues, J. Biomech. 16 (1983) 1–12.
[93] K. Li, R.W. Ogden, G.A. Holzapfel, A discrete fibre dispersion method for excluding fibres under compression in the modelling of fibrous tissues, J. R. Soc. Interface 15 (2018) 20170766.
[94] F. Cosentino, S. Sherifova, G. Sommer, G. Raffa, M. Pilato, S. Pasta, G.A. Holzapfel, Regional biomechanical characterization of human ascending aortic aneurysms: microstructure and biaxial mechanical response, Acta Biomater. 169 (2023) 107–117.
[95] G.A. Holzapfel, R.W. Ogden, Comparison of two model frameworks for fiber dispersion in the elasticity of soft biological tissues, Eur. J. Mech. A Solids 66 (2017) 193–200.
[96] G.A. Holzapfel, R.W. Ogden, Modeling the biomechanical properties of soft biological tissues: constitutive theories, Eur. J. Mech. A Solids 112 (2025) 105634.
[97] P. Hunter, A.D. McCulloch, H. Ter Keurs, Modelling the mechanical properties of cardiac muscle, Prog. Biophys. Mol. Biol. 69 (1998) 289–331.
[98] J. Stålhand, A. Klarbring, G.A. Holzapfel, Smooth muscle contraction: mechanochemical formulation for homogeneous finite strains, Prog. Biophys. Mol. Biol. 96 (2008) 465–481.
[99] A.V. Hill, The heat of shortening and the dynamic constants of muscle, Proc. R. Soc. Lond. B 126 (1938) 136–195.
[100] C.-M. Hai, R.A. Murphy, Cross-bridge phosphorylation and regulation of latch state in smooth muscle, J. Appl. Physiol. 254 (1988) C99–106.
[101] S.-I. Murtada, J.D. Humphrey, G.A. Holzapfel, Multiscale and multiaxial mechanics of vascular smooth muscle, Biophys. J. 113 (2017) 714–727.
[102] G. Franchini, I.D. Breslavsky, F. Giovanniello, A. Kassab, G.A. Holzapfel, M. Amabili, Role of smooth muscle activation in the static and dynamic mechanical characterization of human aortas, PNAS 119 (2022) e2117232119.
[103] A.A. Karkhaneh Yousefi, C. Petit, A.B. Hassine, S. Avril, Stiffness sensing by smooth muscle cells: Continuum mechanics modeling of the acto-myosin role, J. Mech. Behav. Biomed. Mater. 144 (2023) 105990.
[104] A. Giudici, J.M. Szafron, A.B. Ramachandra, B. Spronck, Instability in computational models of vascular smooth muscle cell contraction, Ann. Biomed. Eng. 52 (2024) 2403–2416.
[105] L. Maes, J. Vastmans, S. Avril, N. Famaey, A chemomechanobiological model of the long-term healing response of arterial tissue to a clamping injury, Front. Bioeng. Biotechnol. 8 (2021) 589889.
[106] S.M. Flanary, V.H. Barocas, A structural bio-chemo-mechanical model for vascular smooth muscle cell traction force microscopy, Biomech. Model. Mechanobiol. 22 (2023) 1221–1238.
[107] M. Marino, B. Sauty, G. Vairo, Unraveling the complexity of vascular tone regulation: a multiscale computational approach to integrating chemo-mechano-biological pathways with cardiovascular biomechanics, Biomech. Model. Mechanobiol. 23 (2024) 1091–1120.
[108] S.J. Mousavi, R. Jayendiran, S. Farzaneh, S. Campisi, M. Viallon, P. Croisille, S. Avril, Coupling hemodynamics with mechanobiology in patient-specific computational models of ascending thoracic aortic aneurysms, Comput. Methods Programs Biomed. 205 (2021) 106107.
[109] E.L. Schwarz, M.R. Pfaller, J.M. Szafron, M. Latorre, S.E. Lindsey, C.K. Breuer, J.D. Humphrey, A.L. Marsden, A fluid–solid-growth solver for cardiovascular modeling, Comput. Methods Appl. Mech. Engrg. 417 (2023) 116312.
[110] J.D. Humphrey, K. Rajagopal, A constrained mixture model for growth and remodeling of soft tissues, Math. Models Methods Appl. Sci. 12 (2002) 407–430.
[111] D. Haskett, G. Johnson, A. Zhou, U. Utzinger, J. Vande Geest, Microstructural and biomechanical alterations of the human aorta as a function of age and location, Biomech. Model. Mechanobiol. 9 (2010) 725–736.
[112] A. Corti, M. Colombo, F. Migliavacca, J.-F. Rodriguez Matas, S. Casarin, C. Chiastra, Multiscale computational modeling of vascular adaptation: a systems biology approach using agent-based models, Front. Bioeng. Biotechnol. 978 (2021).
[113] L. Irons, J.D. Humphrey, Cell signaling model for arterial mechanobiology, PLoS Comput. Biol. 16 (2020) e1008161.

[114] E. Nakamachi, T. Uchida, H. Kuramae, Y. Morita, Multi-scale finite element analyses for stress and strain evaluations of braid fibril artificial blood vessel and smooth muscle cell, Int. J. Numer. Methods Biomed. Eng. 30 (2014) 796–813.
[115] A.A. Karkhaneh Yousefi, C. Petit, S. Avril, Stiffness sensing by aortic smooth muscle cells: continuum mechanics modeling of the acto-myosin role, J. Mech. Behav. Biomed. Mater. 144 (2023) 105990.
[116] T.F. Moriarty, The law of Laplace, its limitations as a relation for diastolic pressure, volume, or wall stress of the left ventricle, Circ. Res. 46 (1980) 321–331.
[117] A. Krishnamurthy, C.T. Villongco, J. Chuang, L.R. Frank, V. Nigam, E. Belezzuoli, P. Stark, D.E. Krummen, S. Narayan, J.H. Omens, Patient-specific models of cardiac biomechanics, J. Comput. Phys. 244 (2013) 4–21.
[118] R. Chabiniok, V.Y. Wang, M. Hadjicharalambous, L. Asner, J. Lee, M. Sermesant, E. Kuhl, A.A. Young, P. Moireau, M.P. Nash, Multiphysics and multiscale modelling, data–model fusion and integration of organ physiology in the clinic: ventricular cardiac mechanics, Interface Focus. 6 (2016) 20150083.
[119] R.A. Gray, P. Pathmanathan, Patient-specific cardiovascular computational modeling: diversity of personalization and challenges, J. Cardiovasc. Transl. Res. 11 (2018) 80–88.
[120] M. Peirlinck, F.S. Costabal, J. Yao, J. Guccione, S. Tripathy, Y. Wang, D. Ozturk, P. Segars, T. Morrison, S. Levine, Precision medicine in human heart modeling: Perspectives, challenges, and opportunities, Biomech. Model. Mechanobiol. 20 (2021) 803–831.
[121] I. Mirsky, Left ventricular stresses in the intact human heart, Biophys. J. 9 (1969) 189–208.
[122] D.N. Ghista, K.M. Patil, P. Gould, K. Woo, Computerized left ventricular mechanics and control system analyses models relevant for cardiac diagnosis, Comput. Biol. Med. 3 (1973) 27–46.
[123] M. Sermesant, R. Chabiniok, P. Chinchapatnam, T. Mansi, F. Billet, P. Moireau, J.-M. Peyrat, K. Wong, J. Relan, K. Rhode, M. Ginks, P. Lambiase, H. Delingette, M. Sorine, C. Rinaldi, D. Chapelle, R. Razavi, N. Ayache, Patient-specific electromechanical models of the heart for the prediction of pacing acute effects in CRT: A preliminary clinical validation, Med. Image Anal. 16 (2012) 201–215.
[124] R. Miller, E. Kerfoot, C. Mauger, T.F. Ismail, A.A. Young, D.A. Nordsletten, An implementation of patient-specific biventricular mechanics simulations with a deep learning and computational pipeline, Front. Physiol. 12 (2021) 716597.
[125] R. Piersanti, F. Regazzoni, M. Salvador, A.F. Corno, C. Vergara, A. Quarteroni, 3d–0d closed-loop model for the simulation of cardiac biventricular electromechanics, Comput. Methods Appl. Mech. Engrg. 391 (2022) 114607.
[126] M. Strocchi, C.M. Augustin, M.A. Gsell, E. Karabelas, A. Neic, K. Gillette, O. Razeghi, A.J. Prassl, E.J. Vigmond, J.M. Behar, A publicly available virtual cohort of four-chamber heart meshes for cardiac electro-mechanics simulations, PLoS One 15 (2020) e0235145.
[127] M. Fedele, R. Piersanti, F. Regazzoni, M. Salvador, P.C. Africa, M. Bucelli, A. Zingaro, L. Dede', A. Quarteroni, A comprehensive and biophysically detailed computational model of the whole human heart electromechanics, Comput. Methods Appl. Mech. Engrg. 410 (2023) 115983.
[128] T.P. Usyk, I.J. LeGrice, A.D. McCulloch, Computational model of three-dimensional cardiac electromechanics, Comput. Vis. Sci. 4 (2002) 249–257.
[129] M.P. Nash, A.V. Panfilov, Electromechanical model of excitable tissue to study reentrant cardiac arrhythmias, Prog. Biophys. Mol. Biol. 85 (2004) 501–522.
[130] N.A. Trayanova, Whole-heart modeling: applications to cardiac electrophysiology and electromechanics, Circ. Res. 108 (2011) 113–128.
[131] J.D. Lemmon, A.P. Yoganathan, Three-dimensional computational model of left heart diastolic function with fluid–structure interaction, J. Biomech. Eng. 122 (2000) 109–117.
[132] H. Watanabe, S. Sugiura, H. Kafuku, T. Hisada, Multiphysics simulation of left ventricular filling dynamics using fluid–structure interaction finite element method, Biophys. J. 87 (2004) 2074–2085.
[133] D.A. Nordsletten, S.A. Niederer, M.P. Nash, P.J. Hunter, N.P. Smith, Coupling multi-physics models to cardiac mechanics, Prog. Biophys. Mol. Biol. 104 (2011) 77–88.
[134] A. Santiago, J. Aguado-Sierra, M. Zavala-Aké, R. Doste-Beltran, S. Gómez, R. Arís, J.C. Cajas, E. Casoni, M. Vázquez, Fully coupled fluid-electro-mechanical model of the human heart for supercomputers, Int. J. Numer. Methods Biomed. Eng. 34 (2018) 3140.
[135] D. Chapelle, J.-F. Gerbeau, J. Sainte-Marie, I. Vignon-Clementel, A poroelastic model valid in large strains with applications to perfusion in cardiac modeling, Comput. Mech. 46 (2010) 91–101.
[136] J. Lee, D. Nordsletten, A. Cookson, S. Rivolo, N. Smith, In silico coronary wave intensity analysis: application of an integrated one-dimensional and poromechanical model of cardiac perfusion, Biomech. Model. Mechanobiol. 15 (2016) 1535–1555.
[137] N.A. Barnafi Wittwer, S.D. Gregorio, L. Dede', P. Zunino, C. Vergara, A. Quarteroni, A multiscale poromechanics model integrating myocardial perfusion and the epicardial coronary vessels, SIAM J. Appl. Math. 82 (2022) 1167–1193.
[138] L. Miller, R. Penta, Homogenized multiscale modelling of an electrically active double poroelastic material representing the myocardium, Biomech. Model. Mechanobiol. (2025) 1–28.
[139] B. Marzban, R. Lopez, D.A. Beard, Computational modeling of coupled energetics and mechanics in the rat ventricular myocardium, Physiome J. (2020).
[140] H. Benedicto, P. Bombonato, G. Macchiarelli, G. Stifano, I. Pardo, Structural arrangement of the cardiac collagen fibers of healthy and diabetic dogs, Microsc. Res. Tech. 74 (2011) 1018–1023.
[141] D. Nordsletten, A. Capilnasiu, W. Zhang, A. Wittgenstein, M. Hadjicharalambous, G. Sommer, R. Sinkus, G.A. Holzapfel, A viscoelastic model for human myocardium, Acta Biomater. 135 (2021) 441–457.
[142] W. Zhang, A. Capilnasiu, D. Nordsletten, Comparative analysis of nonlinear viscoelastic models across common biomechanical experiments, J. Elasticity 145 (2021) 117–152.
[143] J.G. Pinto, Y.C. Fung, Mechanical properties of the heart muscle in the passive state, J. Biomech. 6 (1973) 597–616.
[144] J.D. Humphrey, R.K. Strumpf, F.C. Yin, Determination of a constitutive relation for passive myocardium: I, a new functional form, J. Biomech. Eng. 112 (1990) 333–339.
[145] S. Dokos, B.H. Smaill, A.A. Young, I.J. LeGrice, Shear properties of passive ventricular myocardium, Am. J. Physiol. Hear. Circ. Physiol. 283 (2002) 2650–2659.
[146] G. Sommer, A.J. Schriefl, M. Andrä, M. Sacherer, C. Viertler, H. Wolinski, G.A. Holzapfel, Biomechanical properties and microstructure of human ventricular myocardium, Acta Biomater. 24 (2015) 172–192.
[147] D.S. Li, R. Avazmohammadi, S.S. Merchant, T. Kawamura, E.W. Hsu, J.H. Gorman III, R.C. Gorman, M.S. Sacks, Insights into the passive mechanical behavior of left ventricular myocardium using a robust constitutive model based on full 3D kinematics, J. Mech. Behav. Biomed. Mater. 103 (2019) 103508.
[148] S. Kakaletsis, W.D. Meador, M. Mathur, G.P. Sugerman, T. Jazwiec, M. Malinowski, E. Lejeune, T.A. Timek, M.K. Rausch, Right ventricular myocardial mechanics: Multi-modal deformation, microstructure, modeling, and comparison to the left ventricle, Acta Biomater. 123 (2021) 154–166.
[149] J.D. Humphrey, F.C. Yin, A new constitutive formulation for characterizing the mechanical behavior of soft tissues, Biophys. J. 52 (1987) 563–570.
[150] J.D. Humphrey, R.K. Strumpf, F.C. Yin, Determination of a constitutive relation for passive myocardium: II, parameter estimation, J. Biomech. Eng. 112 (1990) 340–346.
[151] J.C. Criscione, A.S. Douglas, W.C. Hunter, Physically based strain invariant set for materials exhibiting transversely isotropic behavior, J. Mech. Phys. Solids 49 (2001) 871–897.
[152] K.D. Costa, J.W. Holmes, A.D. McCulloch, Modelling cardiac mechanical properties in three dimensions, Philos. Trans. R. Soc. Lond. A 359 (2001) 1233–1250.
[153] G.A. Holzapfel, R.W. Ogden, Constitutive modelling of passive myocardium: a structurally based framework for material characterization, Philos. Trans. R. Soc. Lond. A 367 (2009) 3445–3475.
[154] J.M. Guccione, A.D. McCulloch, L.K. Waldman, Passive material properties of intact ventricular myocardium determined from a cylindrical model, J. Biomech. Eng. 113 (1991) 42–55.
[155] O. Gültekin, G. Sommer, G.A. Holzapfel, An orthotropic viscoelastic model for the passive myocardium: continuum basis and numerical treatment, Comput. Methods Biomech. Biomed. Engin. 19 (2016) 1647–1664.
[156] A. Cookson, J. Lee, C. Michler, R. Chabiniok, E. Hyde, D. Nordsletten, M. Sinclair, M. Siebes, N. Smith., A novel porous mechanical framework for modelling the interaction between coronary perfusion and myocardial mechanics, J. Biomech. 45 (2012) 850–855.
[157] P.J. Hunter, A.J. Pullan, B.H. Smaill, Modeling total heart function, Annu. Rev. Biomed. Eng. 5 (2003) 147–177.
[158] J.M. Guccione, G.S. Le Prell, P.P. De Tombe, W.C. Hunter, Measurements of active myocardial tension under a wide range of physiological loading conditions, J. Biomech. 30 (1997) 189–192.
[159] H. Yamashita, S. Sugiura, H. Fujita, S.-I. Yasuda, R. Nagai, Y. Saeki, K. Sunagawa, H. Sugi, Myosin light chain isoforms modify force-generating ability of cardiac myosin by changing the kinetics of actin–myosin interaction, Cardiovasc. Res. 60 (2003) 580–588.
[160] J. Walklate, C. Ferrantini, C.A. Johnson, C. Tesi, C. Poggesi, M.A. Geeves, Alpha and beta myosin isoforms and human atrial and ventricular contraction, Cell. Mol. Life Sci. 78 (2021) 7309–7337.
[161] G. Pardon, H. Lewis, A.S. Vander Roest, O. Chirikian, F. Birnbaum, H. Lewis, E.A. Castillo, R. Wilson, A.K. Denisin, C.A. Blair, C. Holbrook, K. Koleckar, A.C.Y. Chang, H.M. Blau, B.L. Pruitt, Tracking single hiPSC-derived cardiomyocyte contractile function using CONTRAX an efficient pipeline for traction force measurement, Nat. Commun. 15 (2024) 5427.
[162] S.A. Niederer, K.S. Campbell, S.G. Campbell, A short history of the development of mathematical models of cardiac mechanics, J. Mol. Cell. Cardiol. 127 (2019) 11–19.
[163] S. Ranjbarvaziri, K.B. Kooiker, M. Ellenberger, G. Fajardo, M. Zhao, A.S. Vander Roest, R.A. Woldeyes, T.T. Koyano, R. Fong, N. Ma, Altered cardiac energetics and mitochondrial dysfunction in hypertrophic cardiomyopathy, Circulation 144 (2021) 1714–1731.
[164] C. Bountra, R.D. Vaughan-Jones, Effect of intracellular and extracellular pH on contraction in isolated, mammalian cardiac muscle, J. Physiol. 418 (1989) 163–187.
[165] V. Rajagopal, G. Bass, S. Ghosh, H. Hunt, C. Walker, E. Hanssen, E. Crampin, C. Soeller, Creating a structurally realistic finite element geometric model of a cardiomyocyte to study the role of cellular architecture in cardiomyocyte systems biology, J. Vis. Exp. 134 (2018) 56817.

[166] V. Rajagopal, C. Pinali, H.A. Shiels, New revelations on the interplay between cardiomyocyte architecture and cardiomyocyte function in growth, health, and disease: a brief introduction, Phil. Trans. R. Soc. B 377 (2022) 20210315.
[167] L. Asner, M. Hadjicharalambous, R. Chabiniok, D. Peresutti, E. Sammut, J. Wong, G. Carr-White, P. Chowienczyk, J. Lee, A. King, N. Smith, R. Razavi, D. Nordsletten, Estimation of passive and active properties in the human heart using 3D tagged MRI, Biomech. Model. Mechanobiol. 15 (2016) 1121–1139.
[168] J.L. Greenstein, R. Hinch, R.L. Winslow, Mechanisms of excitation-contraction coupling in an integrative model of the cardiac ventricular myocyte, Biophys. J. 90 (2006) 77–91.
[169] J.L. Greenstein, R.L. Winslow, Integrative systems models of cardiac excitation–contraction coupling, Circ. Res. 108 (2011) 70–84.
[170] R. Moss, E.M. Wülfers, S. Schuler, A. Loewe, G. Seemann, A fully-coupled electro-mechanical whole-heart computational model: Influence of cardiac contraction on the ECG, Front. Physiol. 12 (2021) 778872.
[171] J.B. Bassingthwaighte, D.A. Beard, B.E. Carlson, R.K. Dash, K. Vinnakota, Modeling to link regional myocardial work, metabolism and blood flows, Ann. Biomed. Eng. 40 (2012) 2379–2398.
[172] A.S. Vander Roest, C. Liu, M.M. Morck, K.B. Kooiker, G. Jung, D. Song, A. Dawood, A. Jhingran, G. Pardon, S. Ranjbarvaziri, G. Fajardo, M. Zhao, K.S. Campbell, B.L. Pruitt, J.A. Spudich, K.M. Ruppel, D. Bernstein, Hypertrophic cardiomyopathy β-cardiac myosin mutation (p710r) leads to hypercontractility by disrupting super relaxed state, PNAS 118 (2021) 2025030118.
[173] P.M. Cowley, G. Wang, A.N. Chang, D.H. Lovett, J.T. Stull, P.C. Simpson, A.J. Baker, Upregulation of α1a-subtype adrenergic signaling is beneficial in failing right ventricle (RV), Biophys. J. 108 (2015) 293–294.
[174] D.A. Beard, B. Marzban, O.Y. Li, K.S. Campbell, P.M. Janssen, N.C. Chesler, A.J. Baker, Reduced cardiac muscle power with low ATP simulating heart failure, Biophys. J. 121 (2022) 3213–3223.
[175] R. Peyronnet, A. Desai, J.-C. Edelmann, B.A. Cameron, R. Emig, P. Kohl, D. Dean, Simultaneous assessment of radial and axial myocyte mechanics by combining atomic force microscopy and carbon fibre techniques, Phil. Trans. R. Soc. B 377 (2022) 20210326.
[176] C.M. Loescher, J.K. Freundt, A. Unger, A.L. Hessel, M. Kühn, F. Koser, W.A. Linke, Titin governs myocardial passive stiffness with major support from microtubules and actin and the extracellular matrix, Nat. Cardiovasc. Res. 2 (2023) 991–1002.
[177] F. Ježek, A.J. Baker, D.A. Nordsletten, D.A. Beard, Theoretical analysis of power-law stress relaxation and calcium-dependent passive mechanics in cardiac muscle, 2025, http://dx.doi.org/10.1101/2025.02.26.640338, bioRxiv.
[178] S.J. DePalma, J. Jilberto, A.E. Stis, D.D. Huang, J. Lo, C.D. Davidson, A. Chowdhury, M.E. Jewett R.N. Kent III, H. Kobeissi, C.S. Chen, E. Lejeune, A.S. Helms, D.A. Nordsletten, B.M. Baker, Matrix architecture and mechanics regulate myofibril organization, costamere assembly, and contractility in engineered myocardial microtissues, Adv. Sci. 11 (2024) 2309740.
[179] B. López, S. Ravassa, M.U. Moreno, G.S. José, J. Beaumont, A. Gonzalez, J. Díez, Diffuse myocardial fibrosis: mechanisms, diagnosis and therapeutic approaches., Nat. Rev. Cardiol. 18 (2021) 479–498.
[180] A.R. Pinto, A. Ilinykh, M.J. Ivey, J.T. Kuwabara, M.L. D'antoni, R. Debuque, A. Chandran, L. Wang, K. Arora, N.A. Rosenthal, N.D. Tallquist, Revisiting cardiac cellular composition, Circ. Res. 118 (2016) 400–409.
[181] D. Reichart, E.L. Lindberg, H. Maatz, A.M. Miranda, A. Viveiros, N. Shvetsov, A. Gärtner, E.R. Nadelmann, M. Lee, K. Kanemaru, J. Ruiz-Orera, V. Strohmenger, D.M. DeLaughter, G. Patone, H. Zhang, A. Woehler, C. Lippert, Y. Kim, E. Adami, J.M. Gorham, S.M. Barnett, K. Brown, R.J. Buchan, R.A. Chowdhury, C. Constantinou, J. Cranley, L.E. Felkin, H. Fox, A. Ghauri, J. Gummert, R. LI M Kanda, L. Mach, B. MacDonough, S. Samari, F. Shahriaran, C. Yapp, C. Stanasiuk, P.I. Theotakis, F.J. Theis, A. van den Bogaerdt, H. Wakimoto, J.S. Ware, C.L. Worth, P.J.R. Barton, Y.-Ae. Lee, S.A. Teichmann, H. Milting, M. Noseda, G.Y. Oudit, M. Heinig, J.G. Seidman, N. Hubner, C.E. Seidman, Pathogenic variants damage cell composition and single cell transcription in cardiomyopathies, Science 377 (2022) 6606.
[182] S. Nakamori, K. Dohi, Myocardial tissue imaging with cardiovascular magnetic resonance, J. Cardiol. 80 (2022) 377–385.
[183] D.S. Li, E.A. Mendiola, R. Avazmohammadi, F.B. Sachse, M.S. Sacks, A multi-scale computational model for the passive mechanical behavior of right ventricular myocardium, J. Mech. Behav. Biomed. Mater. 142 (2023) 105788.
[184] N. Tueni, J.-M. Allain, M. Genet, On the structural origin of the anisotropy in the myocardium: Multiscale modeling and analysis, J. Mech. Behav. Biomed. Mater. 138 (2023) 105600.
[185] R. Doste, D. Soto-Iglesias, G. Bernardino, A. Alcaine, R. Sebastian, S. Giffard-Roisin, M. Sermesant, A. Berruezo, D. Sanchez-Quintana, O. Camara, A rule-based method to model myocardial fiber orientation in cardiac biventricular geometries with outflow tracts, Int. J. Numer. Methods Biomed. Eng. 35 (2019) e3185.
[186] J. Stimm, D.A. Nordsletten, J. Jilberto, R. Miller, E. Berberoğlu, S. Kozerke, C.T. Stoeck, Personalization of biomechanical simulations of the left ventricle by in-vivo cardiac dti data: Impact of fiber interpolation methods, Front. Physiol. 13 (2022) 1042537.
[187] D. Holz, D. Martonová, E. Schaller, M.T. Duong, M. Alkassar, M. Weyand, S. Leyendecker, Transmural fibre orientations based on laplace–dirichlet-rule-based-methods and their influence on human heart simulations, J. Biomech. 156 (2023) 111643.
[188] C. Von Deuster, E. Sammut, L. Asner, D. Nordsletten, P. Lamata, C.T. Stoeck, S. Kozerke, R. Razavi, Studying dynamic myofiber aggregate reorientation in dilated cardiomyopathy using in vivo magnetic resonance diffusion tensor imaging, Circ. Cardiovasc. Imaging 9 (2016) 005018.
[189] J. Corral-Acero, F. Margara, M. Marciniak, C. Rodero, F. Loncaric, Y. Feng, A. Gilbert, J.F. Fernandes, H.A. Bukhari, A. Wajdan, The 'digital twin' to enable the vision of precision cardiology, Eur. Heart J. 41 (2020) 4556–4564.
[190] S.A. Niederer, M.S. Sacks, M. Girolami, K. Willcox, Scaling digital twins from the artisanal to the industrial, Nat. Comp. Sci. 1 (2021) 313–320.
[191] G. Coorey, G.A. Figtree, D.F. Fletcher, V.J. Snelson, S.T. Vernon, D. Winlaw, S.M. Grieve, A. McEwan, J.Y.H. Yang, P. Qian, P. Qian, K. O'Brien, J. Orchard, J. Kim, S. Patel, J. Redfern, The health digital twin to tackle cardiovascular disease—a review of an emerging interdisciplinary field, NPJ Digit. Med. 5 (2022) 126.
[192] N.A. Trayanova, A. Prakosa, Up digital and personal: How heart digital twins can transform heart patient care, Hear. Rhythm. 21 (2024) 89–99.
[193] J.D. Bayer, R.C. Blake, G. Plank, N.A. Trayanova, A novel rule-based algorithm for assigning myocardial fiber orientation to computational heart models, Ann. Biomed. Eng. 40 (2012) 2243–2254.
[194] S. Klotz, M.L. Dickstein, D. Burkhoff, A computational method of prediction of the end-diastolic pressure–volume relationship by single beat, Nat. Protoc. 2 (2007) 2152–2158.
[195] L.C. Lee, M. Genet, G. Acevedo-Bolton, K. Ordovas, J.M. Guccione, E. Kuhl, A computational model that predicts reverse growth in response to mechanical unloading, Biomech. Model. Mechanobiol. 14 (2015) 217–229.
[196] M. Genet, M. Rausch, L.C. Lee, S. Choy, X. Zhao, G.S. Kassab, S. Kozerke, J.M. Guccione, E. Kuhl, Heterogeneous growth-induced prestrain in the heart, J. Biomech. 48 (2015) 2080–2089.
[197] D. Ambrosi, M. Ben Amar, C.J. Cyron, A. DeSimone, A. Goriely, J.D. Humphrey, E. Kuhl, Growth and remodelling of living tissues: perspectives, challenges and opportunities, J. R. Soc. Interface 16 (2019) 20190233.
[198] E.K. Rodriguez, A. Hoger, A.D. McCulloch, Stress-dependent finite growth in soft elastic tissues, J. Biomech. 27 (1994) 455–467.
[199] J.D. Humphrey, K. Rajagopal, A constrained mixture model for growth and remodeling of soft tissues, Math. Models Methods Appl. Sci. 12 (2002) 407–430.
[200] A.C. Zeigler, A.R. Nelson, A.S. Chandrabhatla, O. Brazhkina, J.W. Holmes, J.J. Saucerman, Computational model predicts paracrine and intracellular drivers of fibroblast phenotype after myocardial infarction, Matrix Biol. 91 (2020) 136–151.
[201] A. Khalilimeybodi, J.J. Saucerman, P. Rangamani, Modeling cardiomyocyte signaling and metabolism predicts genotype-to-phenotype mechanisms in hypertrophic cardiomyopathy, Comput. Biol. Med. 175 (2024) 108499.
[202] C. Sudlow, J. Gallacher, N. Allen, V. Beral, P. Burton, J. Danesh, P. Downey, P. Elliott, J. Green, M. Landray, B. Liu, P. Matthews, G. Ong, J. Pell, A. Silman, A. Young, T. Sprosen, T. Peakman, R. Collins, UK biobank: an open access resource for identifying the causes of a wide range of complex diseases of middle and old age, PLoS Med. 12 (2015) 1001779.
[203] M.I. Kurki, J. Karjalainen, P. Palta, T.P. Sipilä, K. Kristiansson, K.M. Donner, M.P. Reeve, H. Laivuori, M. Aavikko, M.A. Kaunisto, et al., Finngen provides genetic insights from a well-phenotyped isolated population, Nature 613 (2023) 508–518.
[204] A. Sijtsma, J. Rienks, P. Harst, G. Navis, J.G. Rosmalen, A. Dotinga, Cohort profile update: Lifelines, a three-generation cohort study and biobank, Int. J. Epidemiol. 51 (2022) 295–302.
[205] C. Mauger, K. Gilbert, A.M. Lee, M.M. Sanghvi, N. Aung, K. Fung, V. Carapella, S.K. Piechnik, S. Neubauer, S.E. Petersen, A. Suinesiaputra, A.A. Young, Right ventricular shape and function: cardiovascular magnetic resonance reference morphology and biventricular risk factor morphometrics in UK biobank, J. Cardiovasc. Magn. Reson. 21 (2019) 41.
[206] K. Gilbert, W. Bai, C. Mauger, P. Medrano-Gracia, A. Suinesiaputra, A.M. Lee, M.M. Sanghvi, N. Aung, S.K. Piechnik, S. Neubauer, S.E. Petersen, D. Rueckert, A.A. Young, Independent left ventricular morphometric atlases show consistent relationships with cardiovascular risk factors: a UK biobank study, Sci. Rep. 9 (2019) 1130.
[207] M. Santolini, M.C. Romay, C.L. Yukhtman, C.D. Rau, S. Ren, J.J. Saucerman, J.J. Wang, J.N. Weiss, Y. Wang, A.J. Lusis, A.J. Karma, A personalized, multiomics approach identifies genes involved in cardiac hypertrophy and heart failure, NPJ Syst. Biol. 4 (2018) 12.
[208] W.-H. Zimmermann, I. Melnychenko, T. Eschenhagen, Engineered heart tissue for regeneration of diseased hearts, Biomaterials 25 (2004) 1639–1647.
[209] A. Hansen, A. Eder, M. Bönstrup, M. Flato, M. Mewe, S. Schaaf, B. Aksehirlioglu, A. Schwörer, J. Uebeler, T. Eschenhagen, Development of a drug screening platform based on engineered heart tissue, Circ. Res. 107 (2010) 35–44.
[210] E. Tzatzalos, O.J. Abilez, P. Shukla, J.C. Wu, Engineered heart tissues and induced pluripotent stem cells: macro-and microstructures for disease modeling, drug screening, and translational studies, Adv. Drug Deliv. Rev. 96 (2016) 234–244.
[211] J.K. Ewoldt, S.J. DePalma, M.E. Jewett, M.Ç. Karakan, Y.-M. Lin, P. Mir Hashemian, X. Gao, L. Lou, M.A. McLellan, J. Tabares, M. Ma, A.C. Salazar Coariti, J. He, K.C. Toussaint Jr., T.G. Bifano, S. Ramaswamy, A.E. White, A. Agarwal, E. Lejeune, B.M. Baker, C.S. Chen, Induced pluripotent stem cell-derived cardiomyocyte in vitro models: benchmarking progress and ongoing challenges, Nat. Methods 22 (2025) 24–40.

[212] D. Bannerman, S. Pascual-Gil, Q. Wu, I. Fernandes, Y. Zhao, K.T. Wagner, S. Okhovatian, S. Landau, N. Rafatian, D.F. Bodenstein, Y. Wang, T.R. Nash, G. Vunjak-Novakovic, G. Keller, S. Epelman, M. Radisic, Heart-on-a-chip model of epicardial–myocardial interaction in ischemia reperfusion injury, Adv. Heal. Mater. 13 (2024) e2302642.
[213] R.I. Lock, P.L. Graney, D.N. Tavakol, T.R. Nash, Y. Kim, E. Sanchez, M. Morsink, D. Ning, C. Chen, S. Fleischer, I. Baldassarri, G. Vunjak-Novakovic, Macrophages enhance contractile force in iPSC, -derived human engineered cardiac tissue, Cell Rep. 43 (2024) 114302.
[214] J. Moore, J. Ewoldt, G. Venturini, A.C. Pereira, K. Padilha, M. Lawton, W. Lin, R. Goel, I. Luptak, V. Perissi, C.E. Seldman, J. Seldman, M.T. Chin, C. Chen, A. Emili, Multi-omics profiling of hypertrophic cardiomyopathy reveals altered mechanisms in mitochondrial dynamics and excitation–contraction coupling, Int. J. Mol. Sci. 24 (2023) 4724.
[215] M.S. Ma, S. Sundaram, L. Lou, A. Agarwal, C.S. Chen, T.G. Bifano, High throughput screening system for engineered cardiac tissues, Front. Bioeng. Biotechnol. 11 (2023) 1177688.
[216] G. Gut, M.D. Herrmann, L. Pelkmans, Multiplexed protein maps link subcellular organization to cellular states, Science 361 (2018) 7042.
[217] H. Li, S. Sundaram, R. Hu, L. Lou, F. Sanchez, W. McDonald, A. Agarwal, C.S. Chen, T.G. Bifano, Dynamic control of contractile force in engineered heart tissue, IEEE Trans. Biomed. Eng. 70 (2023) 2237–2245.
[218] K. Ronaldson-Bouchard, S.P. Ma, K. Yeager, T. Chen, L. Song, D. Sirabella, K. Morikawa, D. Teles, M. Yazawa, G. Vunjak-Novakovic, Advanced maturation of human cardiac tissue grown from pluripotent stem cells, Nature 556 (2018) 239–243.
[219] S.L. Das, B.P. Sutherland, E. Lejeune, J. Eyckmans, C.S. Chen, Mechanical response of cardiac microtissues to acute localized injury, Am. J. Physiol. Hear. Circ. 323 (2022) 738–748.
[220] N. Thavandiran, N. Dubois, A. Mikryukov, S. Massé, B. Beca, C.A. Simmons, V.S. Deshpande, P. McGarry, C.S. Chen, K. Nanthakumar, G.M. Keller, M. Radisic, P.W. Zandstra, Design and formulation of functional pluripotent stem cell-derived cardiac microtissues, PNAS 110 (2013) 4698–4707.
[221] S. Das, A. Ippolito, P. McGarry, V.S. Deshpande, Cell reorientation on a cyclically strained substrate, PNAS Nexus 1 (2022) 199.
[222] J. Jilberto, S.J. DePalma, J. Lo, H. Kobeissi, L. Quach, E. Lejeune, B.M. Baker, D. Nordsletten, A data-driven computational model for engineered cardiac microtissues, Acta Biomater. 172 (2023) 123–134.
[223] A. Goriely, M.G.D. Geers, G.A. Holzapfel, J. Jayamohan, A. Jérusalem, S. Sivaloganathan, W. Squier, J.A. W. Dommelen, S.L. Waters, E. Kuhl, Mechanics of the brain: perspectives, challenges, and opportunities, Biomech. Model. Mechanobiol. 14 (2015) 931.
[224] H. Oliveri, R. Rooijm, E. Kuhl, A. Goriely, Rheology of growing axons, Phys. Rev. Res. 4 (2022) 033125.
[225] E.K. Pillai, K. Franze, Mechanics in the nervous system: From development to disease, Neuron 112 (2024) 342–361.
[226] H. Oliveri, A. Goriely, Mathematical models of neuronal growth, Biomech. Model. Mechanobiol. 21 (2022) 89–118.
[227] D.E. Koser, A.J. Thompson, S.K. Foster, A. Dwivedy, E.K. Pillai, G.K. Sheridan, H. Svoboda, M. Viana, L. da F. Costa, J. Guck, C. E Holt, K. Franze, Mechanosensing is critical for axon growth in the developing brain, Nat. Neurosci. 19 (2016) 1592–1598.
[228] H. Oliveri, K. Franze, A. Goriely, Theory for durotactic axon guidance, Phys. Rev. Lett. 126 (2021) 118101.
[229] C. Ji, Y. Huang, Durotaxis and negative durotaxis: where should cells go? Commun Biol. 6 (2023) 1169.
[230] M.A. Breau, A. Trembleau, Chemical and mechanical control of axon fasciculation and defasciculation, in: Seminars in Cell & Developmental Biology, Vol. 140, Elsevier, 2023, pp. 72–81.
[231] C. Kassianides, H. Oliveri, A. Goriely, The multiscale mechanics of axon durotaxis, J. Mech. Phys. Solids 200 (2025) 106134.
[232] M.S.H. Joy, D.L. Nall, B. Emon, K.Y. Lee, A. Barishman, M. Ahmed, S. Rahman, P.R. Selvin, M.T. A. Saif, Synapses without tension fail to fire in an in vitro network of hippocampal neurons, Proc. Natl. Acad. Sci. USA 120 (2023) 2311995120.
[233] W.W. Ahmed, T.A. Saif, Active transport of vesicles in neurons is modulated by mechanical tension, Sci. Rep. 4 (2014) 4481.
[234] P. Recho, A. Jerusalem, A. Goriely, Growth, collapse, and stalling in a mechanical model for neurite motility, Phys. Rev. E 93 (2016) 032410.
[235] J.A. García-Grajales, A. Jérusalem, A. Goriely, Continuum mechanical modeling of axonal growth, Comput. Methods Appl. Mech. Engrg. 314 (2017) 147–163.
[236] A. Carnicer-Lombarte, D.G. Barone, F. Wronowski, G.G. Malliaras, J.W. Fawcett, K. Franze, Regenerative capacity of neural tissue scales with changes in tissue mechanics post injury, Biomater. 303 (2023) 122393.
[237] A.E. Forte, S.M. Gentleman, D. Dini, On the characterization of the heterogeneous mechanical response of human brain tissue, Biomech. Model. Mechanobiol. 16 (2017) 907–920.
[238] L.A. Mihai, L. Chin, P.A. Janmey, A. Goriely, A comparison of hyperelastic constitutive models applicable to brain and fat tissues, J. R. Soc. Interface 12 (2015) 20150486.
[239] S. Budday, G. Sommer, C. Birkl, C. Langkammer, J. Haybaeck, J. Kohnert, M. Bauer, F. Paulsen, P. Steinmann, E. Kuhl, Mechanical characterization of human brain tissue, Acta Biomater. 48 (2017) 319–340.
[240] S. Budday, T.C. Ovaert, G.A. Holzapfel, P. Steinmann, E. Kuhl, Fifty shades of brain: a review on the mechanical testing and modeling of brain tissue, Arch. Comput. Methods Eng. 27 (2020) 1187–1230.
[241] L.A. Mihai, S. Budday, G.A. Holzapfel, E. Kuhl, A. Goriely, A family of hyperelastic models for human brain tissue, J. Mech. Phys. Solids 106 (2017) 60–79.
[242] M. Peirlinck, K. Linka, J.A. Hurtado, E. Kuhl, On automated model discovery and a universal material subroutine for hyperelastic materials, Comput. Methods Appl. Mech. Engrg. 418 (2024) 116534.
[243] K. Linka, S.R.S. Pierre, E. Kuhl, Automated model discovery for human brain using constitutive artificial neural networks, Acta Biomater. 160 (2023) 134–151.
[244] S.R. S. Pierre, K. Linka, Kuhl, Principal-stretch-based constitutive neural networks autonomously discover a subclass of Ogden models for human brain tissue, Brain Multiphys. 4 (2023) 100066.
[245] E. Kuhl, A. Goriely, I too i2: A new class of hyperelastic isotropic incompressible models based solely on the second invariant, J. Mech. Phys. Solids 188 (2024) 105670.
[246] A. Goriely, S. Budday, E. Kuhl, Neuromechanics: From neurons to brain, Adv. Appl. Mech. 48 (2015) 79–139.
[247] S. Budday, C. Raybaud, E. Kuhl, A mechanical model predicts morphological abnormalities in the developing human brain, Sci. Rep. 4 (2014) 5644.
[248] D.B. MacManus, M. Ghajari, Material properties of human brain tissue suitable for modelling traumatic brain injury, Brain Multiphys. 3 (2022) 100059.
[249] J. Weickenmeier, P. Saez, C. Butler, P. Young, A. Goriely, E. Kuhl, Bulging brains, J. Elasticity 129 (2017) 197–212.
[250] L. Ronan, N. Voets, C. Rua, A. Alexander-Bloch, M. Hough, C. Mackay, T.J. Crow, A. James, J.N. Giedd, P.C. Fletcher, Differential tangential expansion as a mechanism for cortical gyrification, Cereb. Cortex 24 (2013) 2219–2228.
[251] Z. Wang, B. Martin, J. Weickenmeier, K. Garikipati, An inverse modelling study on the local volume changes during early morphoelastic growth of the fetal human brain, Brain Multiphys. 2 (2021) 100023.
[252] D.H. Barron, An experimental analysis of some factors involved in the development of the fissure pattern of the cerebral cortex, J. Exp. Zool. 113 (1950) 553–581.
[253] G. Xu, A.K. Knutsen, K. Dikranian, C.D. Kroenke, P.V. Bayly, L.A. Taber, Axons pull on the brain, but tension does not drive cortical folding, J. Biomech. Eng. 132 (2010) 071013.
[254] K. Garcia, C. Kroenke, P. Bayly, Mechanics of cortical folding: stress, growth and stability, Philos. Trans. R. Soc. Lond. B Biol. Sci. 373 (2018) 20170321.
[255] M.A. Holland, S. Budday, G. Li, D. Shen, A. Goriely, E. Kuhl, Folding drives cortical thickness variations, Eur. Phys. J. Spec. Top. 229 (2020) 2757–2778.
[256] M. Holland, S. Budday, A. Goriely, E. Kuhl, Symmetry breaking in wrinkling patterns: Gyri are universally thicker than sulci, Phys. Rev. Lett. 121 (2018) 228002.
[257] H. Alawiye, E. Kuhl, A. Goriely, Revisiting the wrinkling of elastic bilayers I: linear analysis, Philos. Trans. A Math. Phys. Eng. Sci. 377 (2019) 20180076.
[258] K.E. Garcia, E.C. Robinson, D. Alexopoulos, D.L. Dierker, M.F. Glasser, T.S. Coalson, C.M. Ortinau, D. Rueckert, L.A. Taber, D.C. Van Essen, C.E. Rogers, C.D. Smyser, P.V. Bayly, Dynamic patterns of cortical expansion during folding of the preterm human brain, Proc. Natl. Acad. Sci. USA 115 (2018) 3156–3161.
[259] K.E. Garcia, X. Wang, C.D. Kroenke, A model of tension-induced fiber growth predicts white matter organization during brain folding, Nat. Commun. 12 (2021) 6681.
[260] L. Del-Valle-Anton, V. Borrell, Folding brains: from development to disease modeling, Physiol. Rev. 102 (2022) 511–550.
[261] N. Traut, K. Heuer, G. Lemaître, A. Beggiato, D. Germanaud, M. Elmaleh, A. Bethegnies, L. Bonnasse-Gahot, W. Cai, S. Chambon, F. Cliquet, A. Ghriss, N. Guigui, A. de Pierrefeu, M. Wang, V. Zantedeschi, A. Boucaud, J. van den Bossche, B. Kegl, R. Delorme, T. Bourgeron, R. Toro, G. Varoquaux, Insights from an autism imaging biomarker challenge: Promises and threats to biomarker discovery, Neuroimage 255 (2022) 119171.
[262] S. Budday, P. Steinmann, A. Goriely, E. Kuhl, Size and curvature regulate pattern selection in the mammalian brain, Extrem. Mech. Lett. 4 (2015) 193–198.
[263] F. Jia, S.P. Pearce, A. Goriely, Curvature delays growth-induced wrinkling, Phys. Rev. E 98 (2018) 033003.
[264] S. Wang, N. Demirci, M.A. Holland, Numerical investigation of biomechanically coupled growth in cortical folding, Biomech. Model. Mechanobiol. 20 (2021) 555–567.
[265] A. Greiner, S. Kaessmair, S. Budday, Physical aspects of cortical folding, Soft Matter 17 (2021) 1210–1222.
[266] N. Demirci, F. Jafarabadi, X. Wang, S. Wang, M.A. Holland, Consistency and variation in the placement of cortical folds: a perspective, Brain Multiphys. 5 (2023) 100080.
[267] J. Weickenmeier, C.A.M. Butler, P.G. Young. A. Goriely, E. Kuhl, The mechanics of decompressive craniectomy: Personalized simulations, Comput. Methods Appl. Mech. Engrg. 314 (2017) 180–195.
[268] J. Weickenmeier, E. Kuhl, A. Goriely, The mechanics of decompressive craniectomy: Bulging in idealized geometries, J. Mech. Phys. Solids 96 (2016) 572–590.

[269] C. Lambride, N. Christodoulou, A. Michail, V. Vavourakis, T. Stylianopoulos, Decompressive craniectomy of post-traumatic brain injury: an in silico modelling approach for intracranial hypertension management, Sci. Rep. 10 (2020) 18673.

[270] M. Sutcliffe, S. Pan, Mechanics of brain tissue deformation and damage following trauma, in: S. Honeybul, A.G. Kolias (Eds.), Traumatic Brain Injury, Springer, Cham, 2021, pp. 19–28.

[271] A.N. Nadzri, N.A. Nik Mohamed, S.J. Payne, M. J. Mohamed Mokhtarudin, Poroelastic modelling of brain tissue swelling and decompressive craniectomy treatment in ischaemic stroke, Comput. Methods Biomech. Biomed. Engin. (2024) 1–11.

[272] J. Kolb, V. Tsata, N. John, K. Kim, C. Möckel, G. Rosso, V. Kurbel, A. Parmar, G. Sharma, K. Karandasheva, S. Abuhattum, O. Lyraki, T. Beck, P. Müller, R. Schlüßler, R. Frischknecht, A. Wehner, N. Krombholz, B. Steigenberger, D. Beis, A. Takeoka, I. Blümcke, S. Möllmert, K. Singh, J. Guck, K. Kobow, D. Wehner, Small leucine-rich proteoglycans inhibit CNS regeneration by modifying the structural and mechanical properties of the lesion environment, Nat. Commun. 14 (2023) 6814.

[273] X. Zhang, J. Weickenmeier, Brain stiffness follows cuprizone-induced variations in local myelin content, Acta Biomater. 170 (2023) 507–518.

[274] C. Kiss, S. Wurth, B. Heschl, M. Khalil, T. Gattringer, C. Enzinger, S. Ropele, Low-frequency MR elastography reveals altered deep gray matter viscoelasticity in multiple sclerosis, Neuroimage Clin. 42 (2024) 103606.

[275] J. Weickenmeier, Exploring the multiphysics of the brain during development, aging, and in neurological diseases, Brain Multiphys. 4 (2023) 100068.

[276] Y. Blinkouskaya, A. Caçoilo, T. Gollamudi, S. Jalalian, J. Weickenmeier, Brain aging mechanisms with mechanical manifestations, Mech. Ageing Dev. 200 (2021) 111575.

[277] M.C. Murphy, D.T. Jones, C.R. Jack Jr, K.J. Glaser, M.L. Senjem, A. Manduca, J.P. Felmlee, R.E. Carter, R.L. Ehman, J. Huston 3rd, Regional brain stiffness changes across the Alzheimer's disease spectrum, Neuroimage Clin. 10 (2015) 283–290.

[278] Y. Feng, M.C. Murphy, E. Hojo, F. Li, N. Roberts, Magnetic resonance elastography in the study of neurodegenerative diseases, J. Magn. Reson. Imaging 59 (2024) 82–96.

[279] A. Goriely, J. Weickenmeier, E. Kuhl, Stress singularities in swelling soft solids, Phys. Rev. Lett. 117 (2016) 138001.

[280] G.E. Lang, P.S. Stewart, D. Vella, S.L. Waters, A. Goriely, Is the donnan effect sufficient to explain swelling in brain tissue slices? J R. Soc. Interface 11 (2014) 20140123.

[281] A. Holmes, P.T. Levi, Y.-C. Chen, S. Chopra, K.M. Aquino, J.C. Pang, A. Fornito, Disruptions of hierarchical cortical organization in early psychosis and schizophrenia, Biol. Psychiatry Cogn. Neurosci. Neuroimaging 8 (2023) 1240–1250.

[282] J.C. Pang, K.M. Aquino, M. Oldehinkel, P.A. Robinson, B.D. Fulcher, M. Breakspear, A. Fornito, Geometric constraints on human brain function, Nature 618 (2023) 566–574.

[283] Y.C. Fung, Biomechanics. Mechanical Properties of Living Tissues, Springer, New York, 1993.

[284] R.W. Ogden, Large deformation isotropic elasticity – on the correlation of theory and experiment for incompressible rubberlike solids, Proc. R. Soc. A 326 (1972) 565–584.

[285] R.W. Ogden, G. Saccomandi, I. Sgura, Fitting hyperelastic models to experimental data, Comput. Mech. 34 (2004) 484–502.

[286] K. Linka, E. Kuhl, A new family of constitutive artificial neural networks towards automated model discovery, Comput. Methods Appl. Mech. Engrg. 403 (2023) 115731.

[287] K. Hornik, M. Stinchcombe, H. White, Multilayer feedforward networks are universal approximators, Neural Netw. 2 (1989) 359–366.

[288] I. Goodfellow, Y. Bengio, A. Courville, Deep Learning, 1st ed., The MIT Press, 2016.

[289] J.A. McCulloch, S.R.St. Pierre, K. Linka, E. Kuhl, On sparse regression, L_p-regularization, and automated model discovery, Internat. J. Numer. Methods Engrg. 125 (2024) e7481.

[290] T. Hastie, R. Tibshirani, J. Friedman, The Elements of Statistical Learning (2nd ed), Springer, New York, 2009.

[291] K. Linka, M. Hillgartner, K.P. Abdolazizi, R.C. Aydin, M. Itskov, C.J. Cyron, Constitutive artificial neural networks: A fast and general approach to predictive data-driven constitutive modeling by deep learning, J. Comput. Phys. 429 (2021) 110010.

[292] D.L. Klein, M. Fernandez, R.J. Martin, P. Neff, O. Weeger, Polyconvex anisotropic hyperelasticity with neural networks, J. Mech. Phys. Solids 159 (2022) 105703.

[293] V. Tac, F. Sahli Costabal, A. Buganza Tepole, Data-driven tissue mechanics with polyconvex neural ordinary differential equations, Comput. Methods Appl. Mech. Engrg. 398 (2022) 115248.

[294] G.A. Holzapfel, K. Linka, S. Sherifova, C. Cyron, Predictive constitutive modelling of arteries by deep learning, J. R. Soc. Interface 18 (2021) 20210411.

[295] S. Kakaletsis, E. Lejeune, M.K. Rausch, Can machine learning accelerate soft material parameter identification from complex mechanical test data? Biomech Model. Mechanobiol. 22 (2023) 57–70.

[296] L.R.G. Treloar, Stresses and birefringence in rubber subjected to general homogeneous strain, Proc. Phys. Soc. 60 (1948) 135–144.

[297] P.J. Blatz, W.L. Ko, Application of finite elastic theory to the deformation of rubbery materials, Philos. Trans. R. Soc. Lond. 6 (1962) 223–251.

[298] M. Mooney, A theory of large elastic deformations, J. Appl. Phys. 11 (1940) 582–590.

[299] R.S. Rivlin, Large elastic deformations of isotropic materials IV. Further developments of the general theory, Phil. Trans. R. Soc. A 241 (1948) 379–397.

[300] H. Demiray, A note on the elasticity of soft biological tissues, J. Biomech. 5 (1972) 309–311.

[301] K. Linka, S.R. St. Pierre, E. Kuhl, Automated model discovery for human brain using constitutive artificial neural networks, Acta Biomater. 160 (2023) 134–151.

[302] J.H. Friedman, Sparse regression in and classification, Int. J. Forecast. 28 (2012) 722–738.

[303] S.L. Brunton, J.P. Proctor, J.N. Kutz, Discovering governing equations from data by sparse identification of nonlinear dynamical systems, Proc. Natl. Acad. Sci. USA 113 (2016) 3932–3937.

[304] M. Flaschel, S. Kumar, L. De Lorenzis, Unsupervised discovery of interpretable hyperelastic constitutive laws, Comput. Methods Appl. Mech. Engrg. 381 (2021) 113852.

[305] T. Bayes, R. Price, An essay towards solving a problem in the doctrine of chances, Philos. Trans. R. Soc. Lond. 53 (1763) 370–418.

[306] K. Linka, G.A. Holzapfel, E. Kuhl, Discovering uncertainty: Bayesian constitutive artificial neural networks, Comput. Methods Appl. Mech. Engrg. 433 (2025) 117517.

[307] H. Holthusen, L. Lamm L, T. Brepols, S. Reese, E. Kuhl, Theory and implementation of inelastic artificial constitutive neural networks, Comput. Methods Appl. Mech. Engrg. 428 (2024) 117063.

[308] M. Flaschel, S. Kumar, L. De Lorenzis, Automated discovery of generalized standard material models with EUCLID, Comput. Methods Appl. Mech. Engrg. 405 (2023) 115867.

[309] S. Avril, M. Bonnet, A.S. Bretelle, M. Grediac, F. Hild, P. Ienny, F. Latourte, D. Lemosse, S. Pagano, E. Pagnacco, F. Pierron, Overview of identification methods of mechanical parameters based on full-field measurements, Exp. Mech. 48 (2008) 381–402.

[310] S. Avril, F. Pierron, General framework for the identification of constitutive parameters from full-field measurements in linear elasticity, Int. J. Solids Struct. 44 (2007) 4978–5002.

[311] S. Avril, S. Evans (Eds.), Material Parameter Identification and Inverse Problems in Soft Tissue Biomechanics, CISM Courses and Lectures, vol. 573, Springer, Cham, Switzerland, 2017.

[312] F. Pierron, M. Grediac, The virtual fields method: Extracting constitutive mechanical parameters from full-field deformation measurements, Springer, New York, 2012.

[313] Y. Mei, S. Avril, On improving the accuracy of nonhomogeneous shear modulus identification in incompressible elasticity using the virtual fields method, Int. J. Solids Struct. 178 (2019) 136–144.

[314] M.R. Bersi, V.A. Acosta Santamaría, K. Marback, P. Di Achille, E.H. Phillips, C.J. Goergen, J.D. Humphrey, S. Avril, Multimodality imaging-based characterization of regional material properties in a murine model of aortic dissection, Sci. Rep. 10 (2020) 1–23.

[315] Z. Zhang, Z. Zou, E. Kuhl, G.E. Karniadakis, Discovering a reaction–diffusion model for alzheimer's disease by combining PINNs with symbolic regression, Comput. Methods Appl. Mech. Engrg. 419 (2024) 116647.

[316] Abaqus Analysis User's Guide, Dassault systèmes simulia corp., Rhode Island, 2024.

[317] M. Peirlinck, K. Linka, J.A. Hurtado, E. Kuhl, On automated model discovery and a universal material subroutine for hyperelastic materials, Comput. Methods Appl. Mech. Engrg. 418 (2024) 116534.

[318] M. Peirlinck, K. Linka, J.A. Hurtado, G.A. Holzapfel, E. Kuhl, Democratizing biomedical simulation through automated model discovery and a universal material subroutine, Comput. Mech. (2024) http://dx.doi.org/10.1007/s00466-024-02515-y.

[319] A.G. Christodoulou, G. Cruz, A. Arami, S. Weingärtner, J. Artico, D. Peters, N. Seiberlich, The future of cardiovascular magnetic resonance: All-in-one vs real-time (Part 1), J. Cardiovasc. Magn. Reson. 26 (2024) 100997.

[320] M.C. Halfmann, S. Bockius, T. Emrich, M. Hell, U.J. Schoepf, G.S. Laux, L. Kavermann, D. Graafen, T. Gori, Y. Yang, R. Kloeckner, P. Maurovich-Horvat, J. Ricke, L. Müller, A. Varga-Szemes, N. Fink, Ultrahigh-spatial-resolution photon-counting detector CT angiography of coronary artery disease for stenosis assessment, Radiology 310 (2024) e231956.

[321] D. Martonová, M. Peirlinck, K. Linka, G.A. Holzapfel, S. Leyendeckera, E. Kuhl, Automated model discovery for human cardiac tissue: Discovering the best model and parameters, Comput. Methods Appl. Mech. Engrg. 428 (2024) 117078.

[322] G.A. Holzapfel, K. Linka, S. Sherifova, Ch.J. Cyron, Predictive constitutive modeling of arteries by deep learning, J. R. Soc. Interface 18 (2021) 20210411.

[323] D. Reinsel, J. Gantz, J. Rydning, Data age 2025 – the digitization of the world from edge to core, 2018, IDC White Paper #US44413318.

[324] S. Samant, J. Bakhos, W. Wu, S. Zhao, G.S. Kassab, B. Khan, A. Panagopoulos, J. Makadia, U.M. Oguz, A. Banga, M. Fayaz, W. Glass, C. Chiastra, F. Burzotta, J.F. LaDisa Jr, P. Iaizzo, Y. Murasato, G. Dubini, F. Migliavacca, T. Mickley, A. Bicek, J. Fontana, N.E.J. West, P. Mortier, P.J. Boyers, J.P. Gold, D.R. erson, J.E. Tcheng, J.R. Windle, H. Samady, F.A. Jaffer, N.R. Desai, A. Lansky, C. Mena-Hurtado, D. Abbott, E.S. Brilakis, J.F. Lassen, Y. Louvard, G. Stankovic, P.W. Serruys, E. Velazquez, P. Elias, D.L. Bhatt, G. Dangas, Y.S. Chatzizisis, Artificial intelligence, computational simulations, and extended reality in cardiovascular interventions, JACC Cardiovasc. Interv. 16 (2023) 2479–2497.

[325] M. Raissi, P. Perdikaris, G.E. Karniadakis, Physics-informed neural networks: A deep learning framework for solving forward, inverse problems involving nonlinear partial differential equations, J. Comput. Phys. 378 (2019) 686–707.

[326] K. Linka, A. Buganza Tepole, G.A. Holzapfel, E. Kuhl, Automated model discovery for skin: discovering the best model, data, and experiment, Comput. Methods Appl. Mech. Engrg. 410 (2023) 116007.

[327] M. Peirlinck, K. Linka, J.A. Hurtado, G.A. Holzapfel, E. Kuhl, Democratizing biomedical simulation through automated model discovery and a universal material subroutine, Comput. Mech. (2024).

[328] C.J. Cyron, J.D. Humphrey, Growth, remodeling of load-bearing biological soft tissues, Meccanica 52 (2017) 645–664.

[329] G.C.Y. Peng, M. Alber, A. Buganza Tepole, W. Cannon, S. De, S. Dura-Bernal, K. Garikipati, G.E. Karniadakis, W.W. Lytton, P. Perdikaris, L. Petzold, E. Kuhl, Multiscale modeling meets machine learning: What can we learn? Arch. Comput. Methods Eng. 28 (2021) 1017–1037.

[330] G.A. Holzapfel, J.D. Humphrey, R.W. Ogden, Biomechanics of soft biological tissues and organs, mechanobiology, homeostasis, and modeling, J. R. Soc. Interface 22 (2025) 20240361.